The Mechanical Design and Analysis of an Active Prosthetic Knee

by

James Lim

A thesis
presented to the University of Waterloo
in fulfillment of the
thesis requirement for the degree of
Master of Applied Science
in
Mechanical Engineering

Waterloo, Ontario, Canada, 2008

I hereby declare that I am the sole author of this thesis. This is the true copy of the thesis, including any required final revisions, as accepted by examiners.

I understand that my thesis may be made electronically available to the public.

James Lim

Abstract

In a world of war and turmoil in developing nations, land mines are becoming a concern, as millions of them are scattered in countries all over the world. Moreover, land mine prevention programs cannot clear land mine fields as fast as they are detonated each day. As a result, there are thousands that fall victim each year.

There is immense demand for newer technologies to replace the aging prostheses used in these war torn nations. The active prosthetic knee (APK) design project is a novel design that utilizes simple, robust one degree of freedom (DOF) mechanics, while providing fully active knee torque control. The APK utilizes a high-speed brushed servomotor, providing the necessary torque and dynamics to provide the necessary gait characteristics of human locomotion.

The main research contributions of this thesis are: 1) the mechanics and 2) the intelligence of the APK. This thesis investigates and highlights the prosthetic's design process. The human biological system is studied and used as the design criteria when designing the device. Anthropometric data was used to determine the sizing and other physical properties. Moreover, Adaptive-Network-based Fuzzy-Interference Systems (ANFIS) and Fuzzy Interference Systems (FIS) are used to provide control to the APK.

Finite element analysis (FEA) verifies the structural integrity of the APK. Four simulations are analyzed: equivalent stress, equivalent strain, shear stress and total deformation. These four simulations provide a mathematical interpretation of the physical system. We found that the first prototype, although a sound design, can be further improved to allow greater loading capabilities. Moreover, cyclical loading and total life cycles would also be significantly improved.

A modular test stand is also designed and prototyped to allow APK testing. Since the APK prototype cannot be immediately placed on a human test subject, the test stand allows for experimentation in replicating human gait cycles.

Acknowledgements

I would like to first thank God for His faithfulness in my life. Being able to build an academic foundation in such a distinguished institution has truly been a blessing and tremendous privilege.

I would like to thank and acknowledge my supervisor and teacher, Dr. William Melek. Thank you William for allowing me to partake in this project. You have encouraged, pushed and taught me through example leadership.

I would also like to thank Dr. Behrad Khamesee for heading this project and also, for allowing me to engage in this multi-faceted project.

I would also like to thank Mr. Roozbeh Borjian, my friend and colleague, for his patience and dedication over the course of this project. Moreover, many thanks to our fourth year students for their endless hours of diligence and significant contributions.

I am indebted to my mother and father for their prayers, support and encouragement. I thank my friends who have continuously pushed me to excel and progress in my studies.

Contents

List of Tables

List of Figures

Nomenclature

Acronyms:

UXO	Unexploded ordnance
CIA	Central Intelligence Agency of the United States of America
ICRC	International Committee of the Red Cross
APK	Active Prosthetic Knee
EMG	Electromyography
DOF	Degrees of Freedom

IC	Initial contact
LR	Loading response
MSt	Mid-stance
TSt	Terminal stance
PSw	Pre-swing
ISw	Initial swing
MSw	Mid-swing
TSw	Terminal swing
ICR	Instantaneous center of rotation
GRF	Ground reaction force

Mathematical Symbols:

r	Moment arm length (in meters)
z_1	Drive gear ratio
z_2	Slave gear ratio
X	Leads (in meters)
α_1	Angle between the ball screw shaft and (in radians)
α_2	Angle between (in radians)
ω_{kr}	Moment arm angular velocity (in revolutions per second)
ω_k	Desired gait angular velocity (in radians per second)
ω_m	Desired motor angular velocity (in radians per second)
ω_{m_rpm}	Desired motor angular velocity (in revolutions per minute)
T_k	Torque output at knee joint (in Newton meters)
T_{k_lbin}	Torque output at knee joint (in pound inches)
T_m	Final output motor torque (in Newton meters)
η_t	Overall system efficiency

Chapter 1

Introduction

1.1 Motivation

In the nation of Afghanistan alone, there are an estimated ten million unexploded ordnance (UXO) devices scattered all throughout the country (ICRC, 2005). These devices were tools to some of the worst war atrocities committed by the Soviet Union throughout its regime over Afghanistan. According to the 2007 data from the United States of America Central Intelligence Agency (CIA, 2008), the population of Afghanistan is 31,889,923. That figure would translate into a ratio of one land mine per three civilians. With such a vast number of land mines still active within various populated areas of the country, the land mine prevention programs are continually, but slowly eliminating such devices - however not fast enough to absolutely rectify the current situation. Each day there are dozens that fall victim to these vicious weapons. According to the International Committee of the Red Cross (ICRC, 2005) of Geneva, since land mine victim relief first started in Afghanistan in 1988, there has been a staggering 72,609 patients. Of these, over 76% of the patients are UXO victims. Although the general trend is a decreasing one, annually there are still thousands of victims losing limbs,

losing jobs, freedom of mobility and increasing difficulty of daily life. One of the greatest hardships for organizations such as the ICRC is that Afghanistan is only one of the multitude of nations that it has to serve. Furthermore, the lower-limb prostheses currently available in these nations would be the yesteryear equivalent of what is deemed viable within the first world. With such crude prosthetics, combined with harsh terrain, such devices are ingredients of difficult patient life. In areas such as North America, western Europe and other privileged nations, there already exists partial and wholly controlled active prosthetic devices able to resemble the likes of human motion. Hence, the motivation of this research is to develop an active prosthetic at a reasonable cost for war victims.

The Active Prosthetic Knee (APK) developed in this thesis is an active device for trans-femoral (above knee) amputees with one amputated leg and one healthy, functioning opposing leg. Most computer based prostheses utilize feedback sensors built into the leg itself and adapts from the dynamic changes it experiences. However, the APK is unique in that the intelligent controller gains information from the opposing healthy leg rather than relying upon sensors built into the prosthetic. The innovation behind its design exemplifies further alternatives and a possible future in intelligent feedback design.

1.2 Research Justification

The notion of mobility is a task that is often taken for granted for the able-bodied. For patients living without a lower-limb, the simple task of executing a stride down a road can take an excruciatingly long time. The daily lifestyle of an amputee in places such as Angola, Vietnam or Afghanistan experience tremendous difficulty in daily life. The mental undertaking, time involved in physiotherapy and all the other processes involved in post amputation is a timely and costly investment. In developing nations, once the amputee is fitted with a prosthetic device, living with it is a tremendous challenges. The precision and accuracy in the fitting process is somewhat crude and heavily compromised when compared to that of the developed world. Numerous visits to the Greater Kabul Area had been made to gather a perspective of the severity of amputee life. It was clearly evident that the lifestyle is extremely difficult to live, as climatic extremes, lack of proper infrastructure suited for the physically

disabled and even cultural discrimination all factor into the hardships endured by many of the physically disabled.

The main focus of this thesis is to design a cost-effective prosthetic knee joint that will allow a full range of motion, comfortable and durable enough to withstand harsh terrain and other physical demands. The *active* in Active Prosthetic Knee refers to the energy being transferred from a power source used to mimic the natural gait cycle. There are three categories of power sources that were considered: hydraulic, pneumatic and electromechanical. As a pragmatic and effective means of active motion, a high-speed, high-powered servomotor was found to be efficient and powerful enough to create the necessary torque to rotate the knee joint.

The Active Prosthetic Knee (APK) is a novel trans-femoral research device that is solely designed in hopes for the physical, societal and personal betterment of amputees of the underdeveloped world. As the underdeveloped world's environment, demographic and general living conditions are usually atrocious, the lack of such devices disables amputees to enjoy the flexibility and ability to enjoy modern biomedical technology that is privy to those living in the modern world.

The greatest challenge in prosthetic design is the user's ability to walk with normal gait. The primary objective in designing those devices is for the prosthetic to mechanically replicate as closely to the subject's natural gait cycle. The APK research and prototype development presented in this thesis, involves the synthesis of a mechanical design and the integration of an intelligent Fuzzy-logic control. The gait cycle can be seen as a simple task, but the study of the dynamics of human locomotion is very complex. By incorporating various forms of feedback control and sensing instruments, the resemblance to real human gait can be realized.

1.3 Literature Review

1.3.1 Lower Body Anatomy

The anatomical three dimensional coordinate system is referred to as the spatial coordinate system, as shown in Figure 1.1. The three coordinates are the sagittal plane, frontal plane and the transverse plane, each corresponding to the X-Y, Y-Z, X-Z global axes respectively. The APK motion study deals predominantly with the sagittal plane, as the large knee movements occur within this plane.

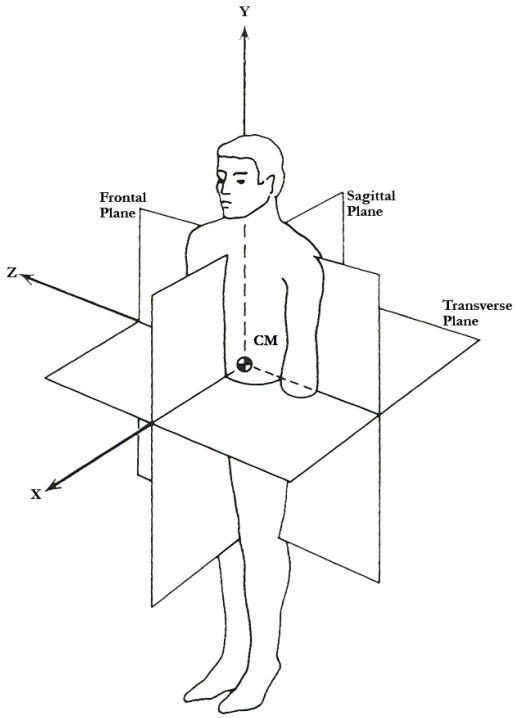

Figure 1.1: Three dimensional anatomical coordinate system (Winter, 2005)

The human skeleton provides six main functions: attachment, blood cell production, movement, protection, shape/support and storage. The attachment function is the tendons and muscles that are fused onto the bone. Ligaments are the connecting points for bones. Furthermore, the bones produces erythrocytes (red blood cells) at the core of the bone, which is also referred to as the bone marrow. The skeletal system is also responsible for the

movement of the body, oftentimes by moving in a hinge-type manner - usually of more than one degree of freedom - combining rotation and translation. One of the key functions of the skeleton is to protect the inner, vital organs such as the brain, eyes and the heart. The hard nature of bones enables protections to these vital and sensitive organs. The skeletal system also provides the shaping and support of the body framework. Lastly, in addition to producing erythrocytes within the marrow, bones also store crucial minerals necessary for the body. Nutrition such as calcium and various vitamins can be stored and released appropriately. There are four main long bones in the lower-limb: the femur, patella, tibia and fibula. The femur bone is the largest and strongest bone, forming at the top with the hip and at the distal end, forms the knee. The amputee who faces an above knee, but below hip amputation, is referred to as a trans-femoral amputee. Hence the user usually requires a stump fitting and a pivoting knee prosthetic to enable stable mobility. Connected to the lower end of the femur is the patella, a flat triangular bone that faces the anterior side of the frontal plane. The cancellous bone structure protects the fine ligaments behind it and also acts as one of the pivoting points of the knee functions. The tibia is one of two bones situated between the femur and the foot. The tibia sits medially and sits adjacent to the fibula. The top called the articular capsule, connected through the lateral condyle and medial condyle is the main interface whereby the six degrees of freedom of the knee rotations are established. The fibula is on the lateral side relative to the tibia and is smaller of the two (as shown in Figure 1.2).

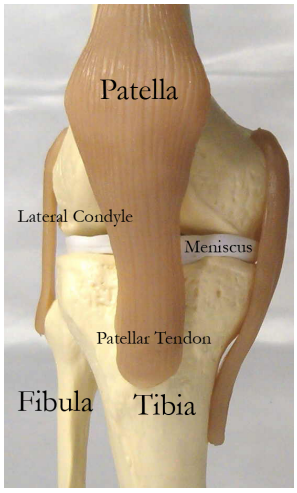

Figure 1.2: Frontal view of the knee joint

1.3.2 Human Locomotion

The walking process can also be referred to as the human gait cycle. Saunders et. al. (1953) defined walking as the translation of the center of mass through space in a manner requiring the least energy expenditure. The gait cycle according to Ayyappa (1997) is the period of time between any two identical events in the walking cycle. The human gait cycle can then be branched off into two sectors, the stance phase and the swing phase. The stance of one side to the stance of the other side is defined as a step, The stance phase of one side to the stance phase of the same side is one full stride. Accordingly, 62% of the human gait cycle (or one full stride) is comprised of the stance phase and the 38% to the swing phase.

Within the swing and stance phases are eight unique branches The stance phase consists of the initial contact (IC), loading response (LR), mid-stance (MSt), terminal stance (TSt) and the pre-swing (PSw). The swing phase consists of the initial swing (ISw), mid-swing (MSw) and the terminal swing (TSw). The direction in which the human walks is referred to as the line of progression. The stride length can be measured between any two consistent points, such as the heel of the same foot. The cadence refers to the number of steps taken per unit of time and is the rate at which a person walks expressed in steps per minute. It differs from velocity in that velocity combines stride length and cadence and is the resultant rate of forward progression. Velocity is the rate of change of linear displacement along the line of progression over a unit of time.

1.3.3 Trans-femoral Prosthetic Mechanical Systems

There are various types of mechanism that are used as trans-femoral amputees. The greatest challenge of trans-femoral prostheses compared to trans-tibial protheses is that the former requires a synthetic knee joint mechanism. These knee joint mechanisms come is various forms. The single axis knee is a relatively simple joint, a simple 1-DOF device. It costs the least and is the most durable with only two moving parts - the femoral segment and the tibial segment. The single axis knee is ideal for remote areas or areas that have limited access to prosthetic care (Blumentritt, 1998). These devices are usually free-swinging and provide no stance control, hence the subject must utilize his or her own muscle power to maintain stability

when walking and standing. More advanced forms of the single axis knee provides constant friction, further allowing limited rotational motion and leads to improved gait efficiency.

The polycentric knees as shown in Figure 1.3, are typically referred to as the "four/five bar" knee, providing multi-axial movement. Polycentric knees provide better stability and locomotion, where the leg's overall length shortens when a step is initiated. This system is well suited for those with knee disarticulation or bilateral amputations (Blumentritt, 1997). Improved and newer versions contain either pneumatic or hydraulic systems allowing variable walking speeds under weight-bearing, whereas the older systems utilize locking mechanisms. Blumentritt et. al. (1997), conducted a comparative study involving polycentric knees with controlled stance features and revealed that newer designs benefitted as they provided varying instantaneous centers of rotations (ICR). However, it cannot replicate the entire range of motion possibly due to the deficiency of the distal insertion of the rectus femoris. Hence the muscles cannot operate as the subject desires. Furthermore, Breakey et. al. (1998), found that as newer systems are becoming more evolved, prosthetists are capable of adjusting the centrode (the path the ICR follows) to allow greater user comfort.

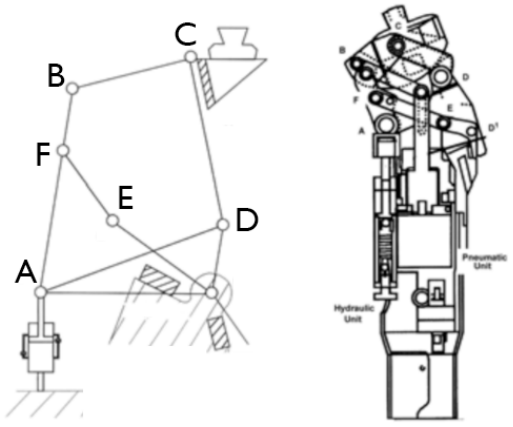

Figure 1.3: An example of a polycentric knee joint

Manual locking knee joints (Figure 1.4) are special in that they lock in leg extension to prevent buckling and stumbling. Although with this sort of device, the user walks a very distorted gait cycle, it is really meant for subjects who are weaker.

Figure 1.4: A manual locking prosthetic knee joint (Otto, 2003)

Constant friction systems offer a form of linear, constant mechanical friction at the axis of rotation and adjust to match the normal cadence of the opposite leg. However, one major drawback is that these units typically operate when the user's walking speed is constant (steady-state gait).

Variable friction motion controlled devices are slightly different in that they provide increased resistance as the knee bends from full extension. This unique characteristic is referred to as "cadence response", which solves the deficiencies experienced by the constant friction device, by allowing comfort during variable walking speeds. However, the drawback of the variable system is the advanced engineering of the device, resulting in complex internal fluid vanes that can break and are costly to maintain and repair. Therefore, maintenance is crucial because of the system's fragile nature, if not cared for regularly. Fully pneumatic and hydraulic prostheses utilize fluid dynamics to provide variable resistance, allowing the user to walk comfortably at varied speeds.

Pneumatic control compresses air as the knee is flexed, storing energy, then returning the energy as the knee enters into extension. Similarly, hydraulic devices utilize a liquid medium (typically of silicone oil) as opposed to air in order to respond to a greater range of walking

speeds. The hydraulic systems typically cost more and are heavier and require more maintenance. More advanced, modern systems have built into them a hydraulic terminal impact dampener, which allows for a gentle motion in the swing phase. Blumentritt et. al. (1999) of Otto Bock Orthopadische Industrie GmbH have investigated the various gait cycles of subjects on rotary hydraulic devices (Figure 1.5) and found that the rotary design is wholly dependent on the ground reaction force (GRF) exerted from the user.

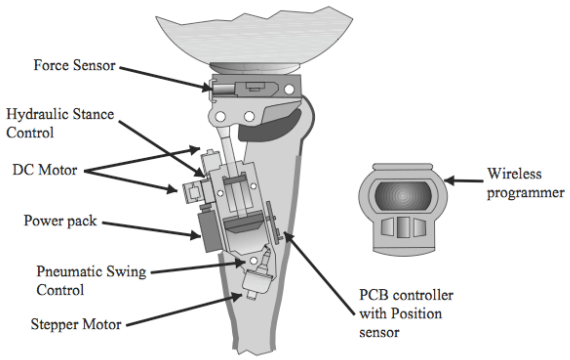

Figure 1.5: A pneumatic prosthetic (Zahedi, 2005)

Lastly, the microprocessor controlled prosthetic as shown in Figure 1.6 is the latest and most advanced in the broad array of modern trans-femoral prostheses. Processors built into the leg allow feedback from a variety of sensors that measures attributes such as speed, acceleration, yaw and pitch. The processor is able to sense various terrain and gait properties and adjusts the pneumatic and/or hydraulic systems to allow for greater user comfort and ease.

Figure 1.6: The Otto Bock microprocessor C-Leg (Otto Bock, 2007)

1.3.4 Current Research

Investigative research in academia and industry reveals the broad range of developmental and testing progress of trans-femoral prostheses, especially in the aspect of gaining efficiency through improved designs and also with powered systems.

Boonstra et. al. (1995), have been involved with the study in gait efficiency of trans-femoral amputees. By testing various subjects with varying knee designs, their study would record heart rate through telemetry and measure expired gas exhaled by the user. Buckley et. al. (1997) looked into a comparative study of a conventional pneumatic swing control system to an intelligent prosthesis and found that by combining an "intelligent" processor, gait efficiency increased by 4.1%. It was also determined by Gitter et. al. (1997), that the mass of the prosthetic in the swing phase had negligible effect on the efficiency - only investigating the oxygen consumption of the test subjects. Similarly, Godfrey et. al. (1977), conducted a study investigating the weight of the prosthetic foot and its effects as a swinging moment mass and found that varying prosthetic masses resulted in negligible differences.

Greene et. al. (2003), investigated a design study for paraplegics, utilizing a cam-based design and customized for specific users in rehabilitation. There is a tremendous effort in the development of biomechanical exoskeletons (Zoss, 2006), not for amputees, but for improved combat use. These adaptable mechanical designs follow the same principles as trans-femoral prosthetic design, however, crucial are the aspects of power storage and design engineering methods in packaging. More relevant are studies conducted by Kapti et. al. (2006), in Turkey, where it is found that a fully powered trans-femoral joint is necessary as gait efficiency and user energy are depleted by using passive and semi-active devices. Saito et. al. (2005), have investigated the topic of lower-limb prostheses powered by servo pneumatic actuators. By utilizing master and slave cylinders, they have created a novel system to maximize efficiency by prudent energy savings. Zoss and Kazerooni (2006) also utilized a gas/hydrogen peroxide based fuel cell to create a high intensity battery with long hours of operation.

1.4 Research Contributions

The Active Prosthetic Knee is a design innovation that is a result of the recognized need and urgency of newer, evolving prosthetic technologies in the developing world. This research focuses on two crucial aspects. The first is the mechanical durability that allows subjects to use a leg for extended periods of time in harsh geographic settings, without the inconvenience of short term maintenance. Secondly, the most significant portion of the research aspect is the feedback control system, and the APK ability to closely resemble human locomotion.

Mechanics of the APK

The mechanics of the APK involves the design of an overall system with five degrees of freedom (DOF), where the actual knee joint in isolation is one degree of freedom. The motivation behind the single pivoting mechanism is primarily due to the focus of a low-cost device, where a single pivoting point decreases the number of parts used and allows for greater durability. Although single DOF knee joints are the least accurate in terms of mimicking locomotion relative to the more advanced systems, the initial intelligent system is far simpler to control a reduced DOF motion. The APK prototyping stage provided insight as each design was re-designed and variants were created thereafter. The result is an almost all aluminum design that is modular, hence allowing an open architecture concept. The concept of an open architecture provides flexible mechanical changes such as gearing and motor selection that is best suited for a certain demographic.

Intelligence of the APK

The second aspect of the research contribution involves the novel design of intelligent feedback control utilizing the healthy leg's electrical impulses from EMG sensors, angle sensors and accelerometers from gait dynamics. The user will have sensors attached to the healthy leg, and different signals from the healthy leg's motion will be sent to the micro-controller. The micro-controller then sends signals to a servo motor varying torque and rotational speed commands that will prompt the leg to move accordingly. The output motor movements recorded by an encoder will then be sent back to adjust the control command with the purpose of closely following a normal gait walking patter.

The overall system is unique in that its open architecture of mechanical flexibility allows for easier maintenance and accessibility. If the subject is an adolescent, the flexibility allows various gearing ratios as well as height adjustments to allow for a broader height margin. The purpose of this conceptual design is to allow developing world war victims to experience improved efficiency in gait energy by assistive motors. This allows greater accessibility through intelligent design for simple maintenance and long-term use.

1.5 Thesis Organization

This thesis documents a collaborative investigation of human locomotion and the process of converting the gait cycle into a cost-effective mechanical system that provides full active knee torque for transfemoral amputees.

Chapter 2 covers with the design methodology of the APK system. It involves the design and development stages of the mechanical functions of the APK. Range of motion of the human leg and its vast complexity when interpreting it mechanically is also detailed. Furthermore, the design process for the prototype is also presented in details.

Chapter 3 investigates the Finite Element Analysis (FEA) study, exploring the physical aspects; strength as well as the weaknesses of the APK's structural integrity. A key section investigates a full stance phase of the entire gait cycle. The chapter provides a visual representation of the stresses acting on the major components of the prosthetic.

Chapter 4 covers in brief, the controller design. It investigates the algorithmic development of the Adaptive-Network-based Fuzzy-Interference System (ANFIS) and the Fuzzy Interference System (FIS).

Chapter 5 covers the design of the test stand and pneumatic circuit that simulates the femoral movements. The chapter looks into the design stages for prototype fabrication.

Finally, Chapter 6 provides the conclusions of the thesis and accounts for recommendations for future academic and commercial endeavors.

Chapter 2

Model Development

2.1 Introduction

Throughout the prototyping and testing stage of the Active Prosthetic Knee (APK), it was found that the development of artificial limbs is a tremendous engineering feat. The primary concern is the prosthesis' ability to move and perform closely resembling that of natural lower-limb motor movements. Factors such as range of motion, angular speed, flexibility and energy transfer all attribute to overall user comfort and efficiency of the prosthetic. Moreover, in recent commercial lower-limb prosthetic endeavors, costs have surged to the point where many underprivileged in developing countries or uninsured households cannot afford these devices. Costs of active prostheses can equivalent yearly household incomes. It is therefore, significantly difficult, if not impossible for developing world war victims to afford and make use of these devices.

2.2 Human Compatibility

Since the APK is a non-invasive device, biomaterial compatibility is not a concern. There are several material qualities that are necessary to allow the APK to withstand harsh environments. There are several material considerations, where constraints such as weight versus durability comes into play. The APK must be light and agile enough to allow prolonged use by the user. However, people in developing nations typically walk over more rugged terrain and long walking distances for prolonged durations requires mechanical maneuverability as well as extreme durability. The tradeoff with lighter, stronger materials results in increased costs. As the component of low-cost is the core driving focus of the APK, unique solutions are a necessity.

2.2.1 Anthropometric Analysis

The APK's modular architecture design allows fitment for a broad demographic range. Anthropometrics is the study of human body measurements, investigating size, length and mass proportions to use in anthropological studies (Winter, 2005). The APK prototype is based on North American stature demographics, strictly for testing purposes. The purpose of these measurements is to build a device to allow testing compatibility for laboratory purposes. The APK is designed to be utilized by the 5th to 95th percentiles of 20 year-old males in the United States between 165 centimeters to 189 centimeters (CDC Growth Charts, 2000). The 50th percentile is 177 centimeters. For the prototype, the data is based on research conducted at the University of Waterloo's Department of Kinesiology. The data acquired is based on a non-amputated male test subject of 56.7 kg and height of 172 cm. The subject's leg segment length of 42.5 cm is defined to begin from the lateral epicondyle of the thigh (knee) down to the lateral malleolus (ankle) of the right leg, as shown in Figure 2.1. The APK's unique design allows for a broad range of user sizes, however optimized (in this case) for the aforementioned demographic range. Although leg segment lengths vary between individuals, utilizing anthropometric data allows the APK's dimensions to be designed for use by a large demographic range.

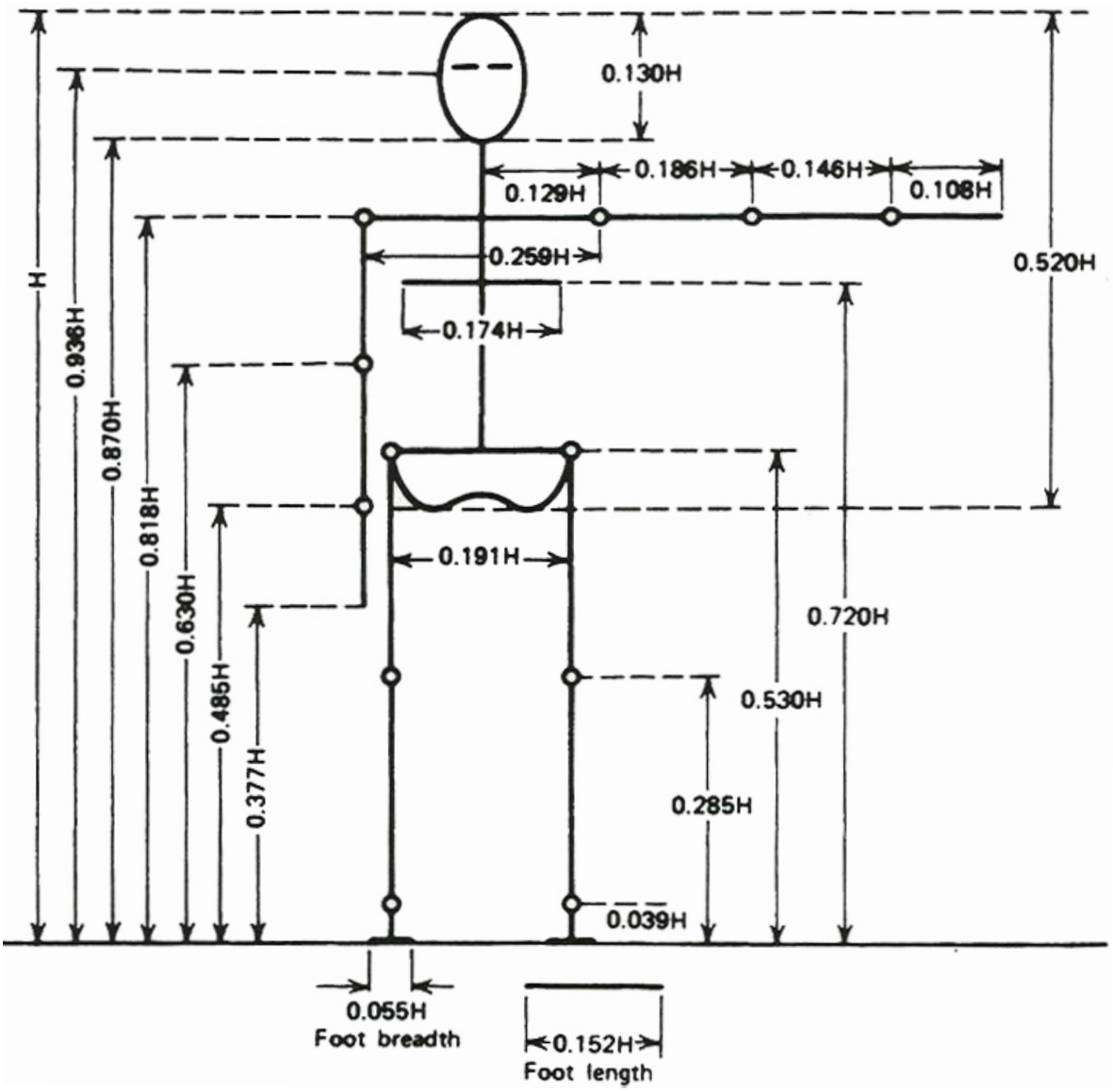

Figure 2.1: Anthropometric data for a skeletal system (Winter, 2005)

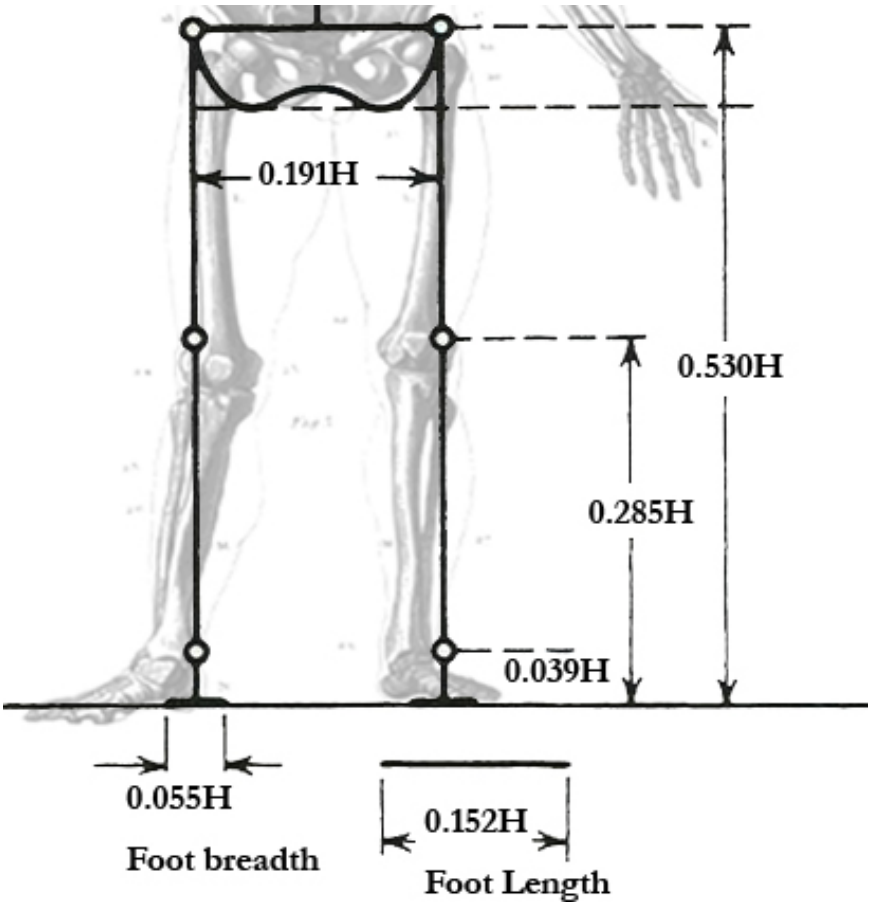

Figure 2.2: Anthropometric data for the lower body (Winter, 2005)

The variable *H* is the overall height of the subject. The tibial proportion measures 0.246*H*, equating to a length range of 0.406 m to 0.465 cm and an average length of 0.435 cm (as shown in Figure 2.2). The total length of the APK is 0.275 m long, allowing adequate fitment for users at statures of 110 cm or more.

Another critical component of anthropometric data, is the weight variation, that will disallow it from fitting as broad a demographic range, based on height alone. Derived from anthropometric charts (Winter, 2005), the leg segment is defined as the solid link between the femoral condyles (knee) to the medial malleolus (ankle). The segment's weight, much like the height, is an average fixed fraction of total body weight. The segment weight of the leg is

0.0465 *M*, where *M* is the total weight of the entire body. For the prototyping process, the subject weight used is 56.7 kg. This member is found to be 2.63 kg. The APK's total weight is 1.63 kg, nearly one kilogram lighter than the anatomical leg, allowing a balanced symmetry (with a tibial and foot extension) in weight and overall motion dynamics.

2.2.2 Range of Motion and Knee Mechanics

The motion of human systems is a complex one; it is difficult for an engineered devices to accurately replicate natural gait. The knee joint is a complex mechanism consisting of six degrees of freedom, in various rotating and translating motions (Fujie, 1996). To mechanically design and allow an engineered device to move in this fashion requires tremendous mechanical complexity and with weight and budgetary limitations, realistically cannot be realized.

Figure 2.3 represents a normal walking cycle, where there are two distinct aspects, the stance phase and the swing phase. The stance phase is when the foot in is contact with the ground surface, and the swing phase is when the foot is not in contact with any ground surface. Since the events for each person occurs in a similar sequence but varies with respect to time, the gait cycle can be described in terms of percentage, allowing normalization of the data for multiple subjects. By definition, the initial foot strike occurs at 0%, and the second foot strike at 100%. The opposite leg undergoes the same events, but are out of phase by 180 degrees, with the opposite foot strike representing the 50% mark (Ayyappa, 1997). Stance is the period when the foot is in contact with the ground and constitutes 62% of the gate cycle. The remaining 38% of the gait cycle constitutes the swing period that is initiated as the toe leaves the ground. There are also four phases within the stance phase: *initial double support, mid-stance*, *terminal stance*, and *second double support.* The initial limb support is characterized by a very rapid weight acceptance onto the forward limb with shock absorption and slowing of the body's forward momentum. Mid-stance (phase #2) and terminal stance (phase #3) are involved in the task of single limb support when the weight of the body is fully supported by the reference limb (from opposite toe-off to opposite foot strike). The second double support (phase #4), which is also called pre-swing, prepares the limb to swing. The transfer of body weight from the reference limb to the opposite limb takes place in this stage. The swing period can be subdivided into three phases: *initial swing, mid-swing, and terminal swing.* Initial swing (phase #5)

starts with toe-off and ends with foot clearance when the swinging foot is opposite the stance foot. Mid-swing (phase #6) continues from the end point of the initial swing and continues until the swinging limb is in front of the body and the tibia is vertical. In the terminal swing (phase #7), the limb decelerates and strikes the ground for the second time. Limb advancement is performed during the pre-swing phase and throughout the entire swing period.

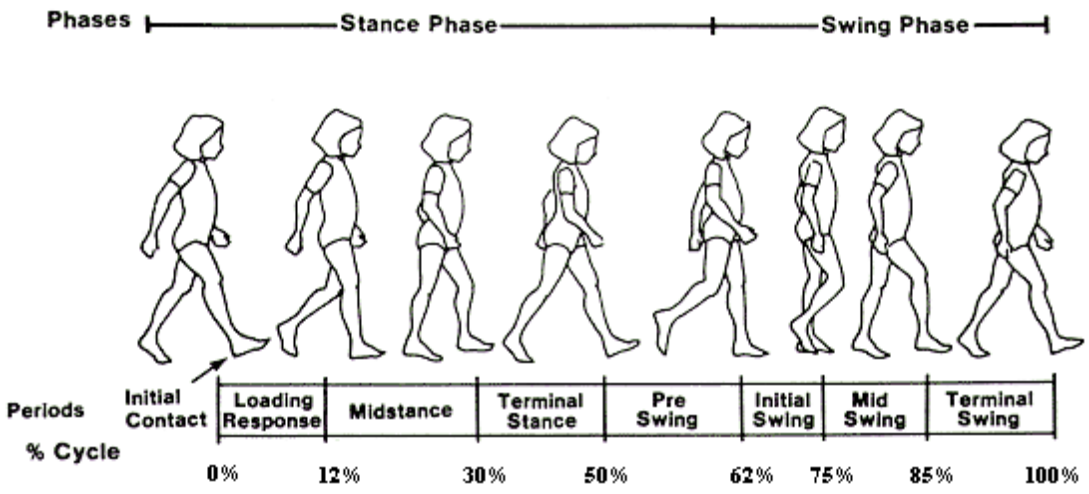

Figure 2.3: The phases of a gait cycle

The gait cycle for an adult male with a single transfemoral prosthetic amputation, weighing 69 kg and stature of 179 cm is between 1.07 m/s and 1.26 m/s at a slow walking pace (Van Der Linden, 1999). During a slightly faster gait cycle, the subject travels at a steady-state velocity of 1.48 m/s to 1.59 m/s. Each stride (defined as one full walking cycle) is 1.58 m to 1.75 m in length. Figure 2.4 presents a stick diagram that represents link segments from marker data placed on joints, while the subject is walking.

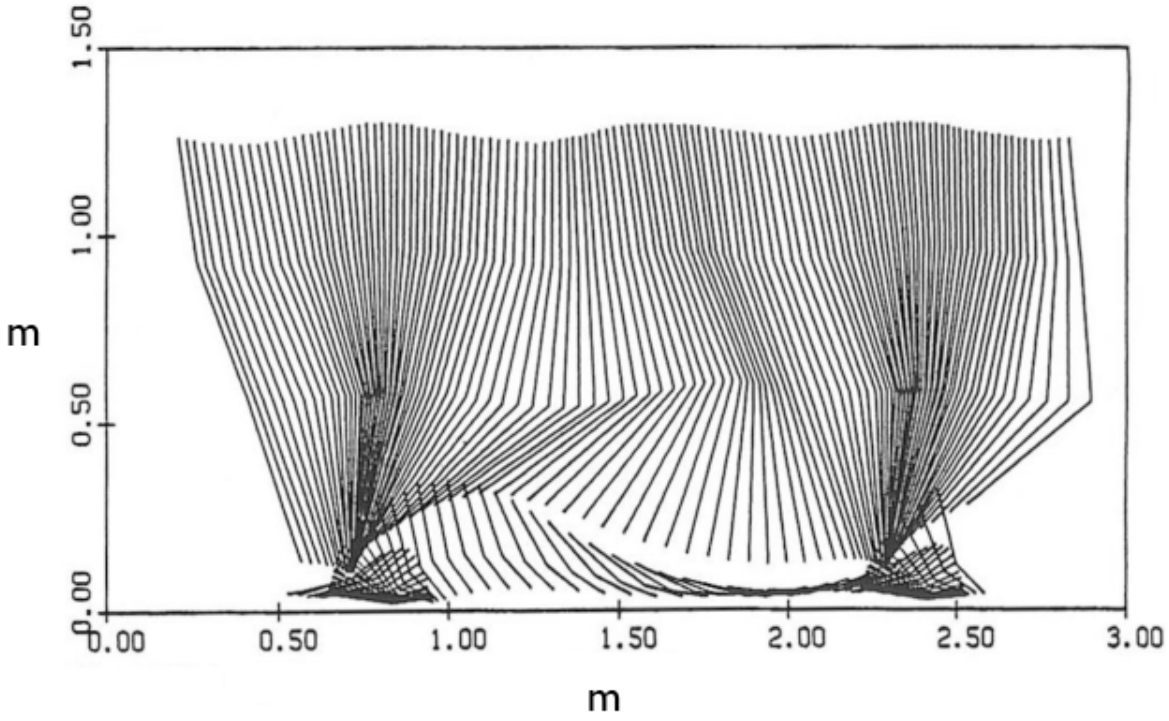

Figure 2.4: Stick diagram of walking gait cycle (Winter, 2005)

The knee joint can be seen as a simplified kinematics system, where the anatomical makeup reveals the functions of the joint. The Link-Segment Model (LSM) looks at the segment masses, centers of mass, joint centers and moments of inertia to calculate the joint properties (Winter, 2006).

Figure 2.5 represents the free body diagram of any arbitrary joint in the human body. In this example, F_{j1} and F_{-j2} are joint forces of the same magnitude but opposite direction. V_{-j} corresponds to both joints with the same linear velocity. Lastly, θ_1 and θ_2 represent the angle between the force and velocity.

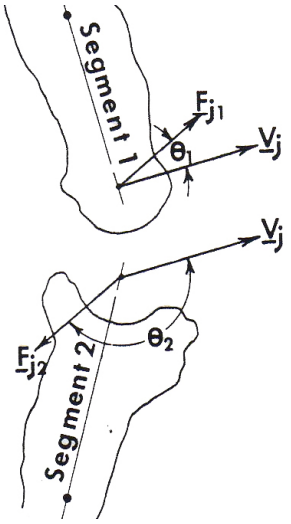

Figure 2.5: Free body diagram of an arbitrary joint (Winter, 2005)

Using external kinematic, kinetic and anthropometric data, internal factors can be found. Joint reaction forces, net muscle moments and kinetic as well as potential energy can be calculated. The link segment model essentially breaks down each leg component by using the conservation of energy and momentum, determining the internal components. There are three contributing forces that act on the LSM: gravitational forces, ground reaction forces (GRF)/external forces and muscle/ligament forces. First, the gravitational component is the force that accelerate the mass at a magnitude of 9.81 m/s^2. Secondly, ground reaction and external forces are components from which the body experiences from factors external to the anatomical system. These would include forces experienced by the body due to the normal force acting on the foot. Thirdly, the muscle and ligament forces are what allows the motor movements to occur.

Knee motion information is processed with reference to normalized gait cycle. The knee joint angular velocity to percentage cycle reveals that the leg undergoes the largest angular velocity at 87% of the gait cycle, as the leg is in swing phase and approaches heel strike (Figure 2.6). Figure 2.7 shows that the knee's total angular range of motion is 60°. In contrast, in the knee

joint torque graph as shown in Figure 2.8, the greatest torque is experienced at 15%, where 36 Nm is exerted on the knee joint as the leg undergoes the mid-stance phase (refer Appendix B).

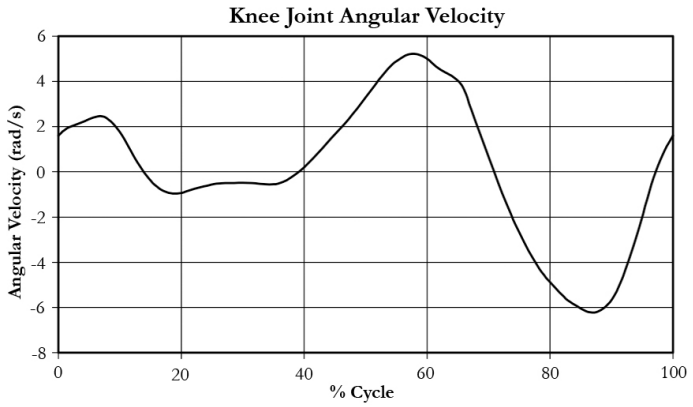

Figure 2.6: Knee joint angular velocity versus gait cycle (Winter, 2005)

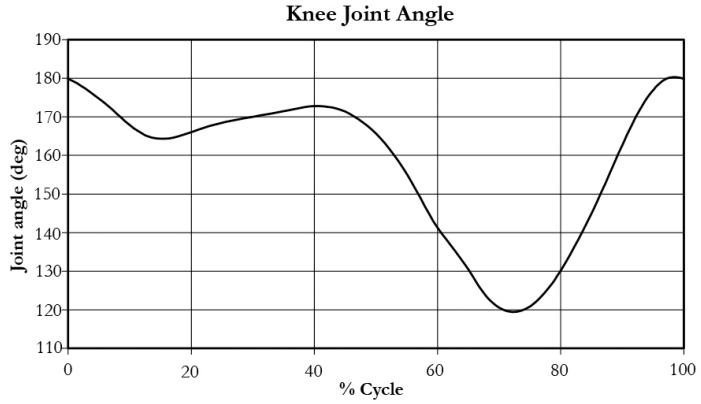

Figure 2.7: Knee joint angle versus gait cycle (Winter, 2005)

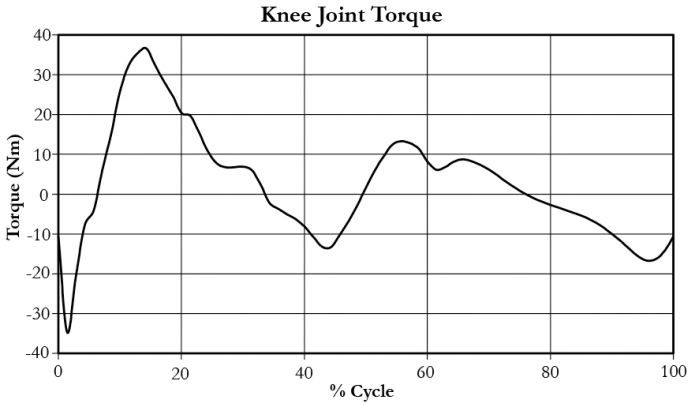

Figure 2.8: Knee joint torque versus gait cycle (Winter, 2005)

The anatomical knee joint is a 6-DOF system, which includes a series of sliding and rotating motions. The six different degrees of freedom (as shown in Figure 2.9) are comprised of extension-flexion (E-F) rotation (θ_{EF}), varus-valgus (V-V) rotation (θ_{VV}), internal-external (I-E) rotation (θ_{IE}), lateral-medial (L-M) translation (d_{LM}), anterior-posterior (A-P) translation (d_{AP}) and proximal-distal (P-D) translation (d_{PD}) (Fujie, 1996). These six unique movements of rotation and translation indicate the complex knee system.

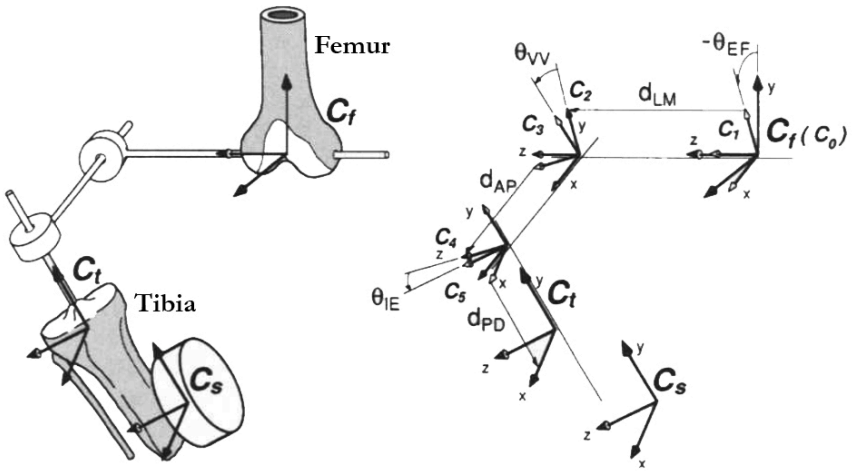

Figure 2.9: Six degrees of freedom of the knee joint (Fujie, 1996)

One group of researchers has found the range of motion corresponding to the rotations and translations about the knee. In their study, they examined 42 men of 169 cm ± 6 cm, where each would walk at a similar pace over the same distance. The extension-flexion limit was found to be 54.1° ± 9.9° and the angles for the external-internal rotation experiences a total range of motion of 12.4° ± 4.5°. The varus-valgus rotation was found to be 8.2° ± 3.6°. Thetranslation components were found as adduction-abduction at 6.5 mm ± 4 mm, anterior-posterior to be 11.5 mm ± 5 mm and the lateral-medial translation as 4 mm ± 3.5 mm. The APK's mechanical development is based on a simplified platform, where the major rotations are taken into consideration. The translational motions are not considered, as the APK focus of being simple and robustness is the key focal point. Table 2.1 presents each rotation and translation.

Table 2.1: Degrees of Freedom of anatomical knee

Type of Motion	*Rotation*	*Rotation*	*Rotation*	*Translation*	*Translation*	*Translation*
Name of DOF	Extension-Flexion	External-Internal	Varus-Valgus	Adduction-Abduction	Anterior-Posterior	Lateral-Medial
Angle/ Distance	54.1° ± 9.9°	12.4° ± 4.5°	8.2° ± 3.6°	6.5 ± 4 mm	11.5 ± 5 mm	4 ± 3.5 mm

The APK is a simplified knee joint, a system with 5-DOF, while the knee joint in isolation is 1-DOF (discussed in the next section). The knee joint can experience a total range of extension-flexion motion of 90°. Furthermore, the APK design incorporates 1-DOF at the knee joint, making the prototype simple to control and cost effective.

2.3 Mechanical Design Stages

2.3.1 Design Criterion

The design process of the APK took three major forms, where three iterations and redesigns took place sequentially to create the final prototype. The focus of a broad demographic range fitment and mechanical rigidity influenced the design of the APK. The design philosophy was

to create the APK in keeping with the anatomical system, but also abiding by the objective of minimal weight and cost. The prototype device is almost wholly fabricated from aluminum 6061. The femoral socket is not considered, as the APK is strictly a transfemoral (below-knee to above ankle) knee joint with a tibial extension.

The most prominent component of the APK is the tibial component, which the largest and the one that handles the greatest loads. The actual design of the APK is engineered in such a way that high stresses and high impact would not cause deformation of the aluminum. Also, the APK must exhibit tremendous rigidity to withstand the rigorous terrain of developing areas. The main tibial component as shown in Figure 2.10, is in the form of an arch to resist compression in the frontal plane, and to promote greater stress resistance in the transverse plane.

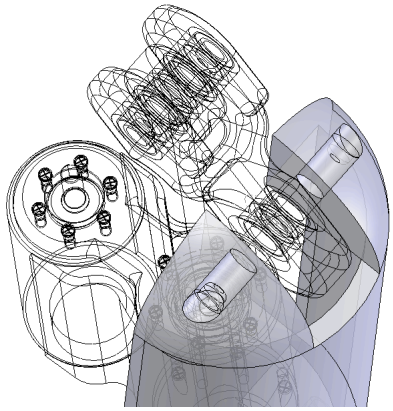

Figure 2.10: Tibial shell

Each of the 1-DOF moving components are dual, steel enclosed, high-precision bearings in parallel arrangement for greater torsional stability. The 2-DOF ball-screw device is a high-speed, austenitic-chromium-nickel-manganese 202 stainless steel. The overall prototype system is based upon a 2000 N of applied dynamic force, replicating approximately that of a 70 kg subject with a multiplication factor of three - replicating a fast gait.

Figure 2.11 highlights each of the main components of the APK. Distal to the knee joint, is the structural carrier component (1), that takes the load bearing of the entire system above it.

The tibia (2) is the frontal component of the APK and is connected to the torque arm (3) that provides the necessary power to the knee joint. The ball-screw system (4) is housed within the motor carrier (5). Figure 2.12 shows an exploded three dimensional view of all the APK components and Figure 2.13 presents views of the the design. Figures 2.14, 2.15 and 2.16 are images of the actual APK prototype model.

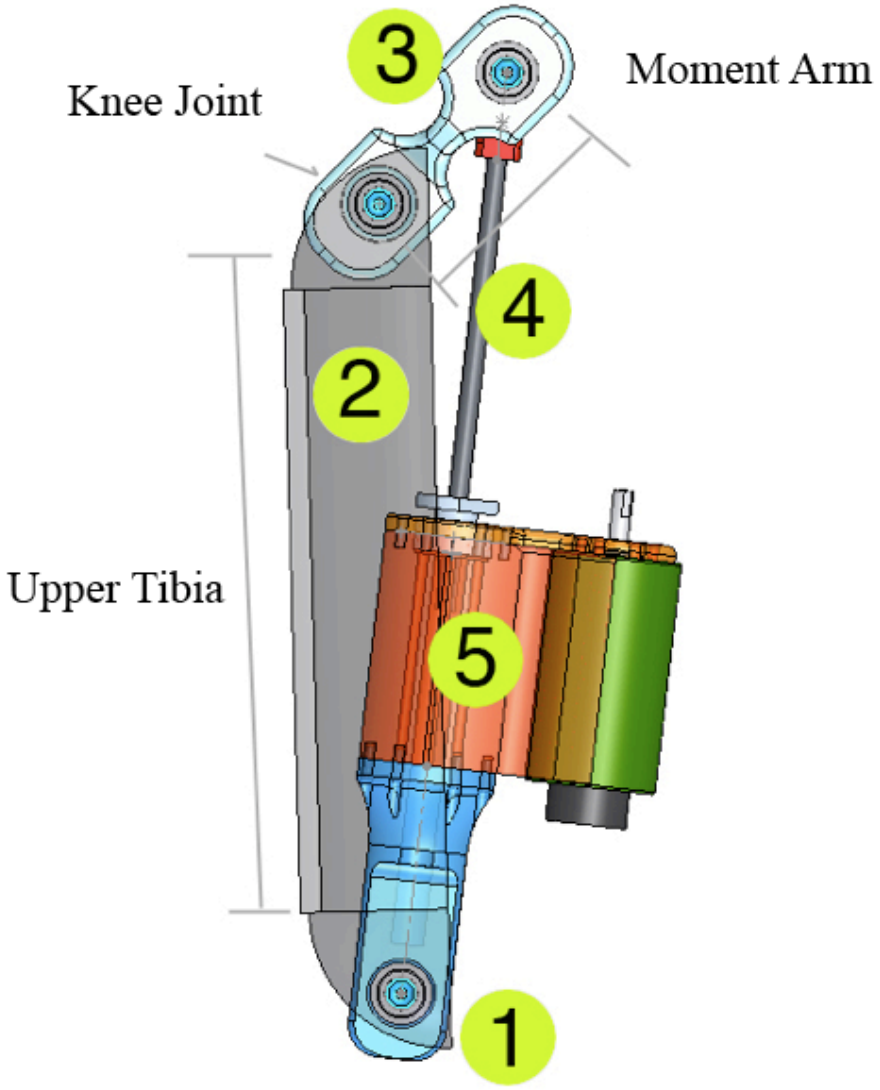

Figure 2.11: Profile view of the APK

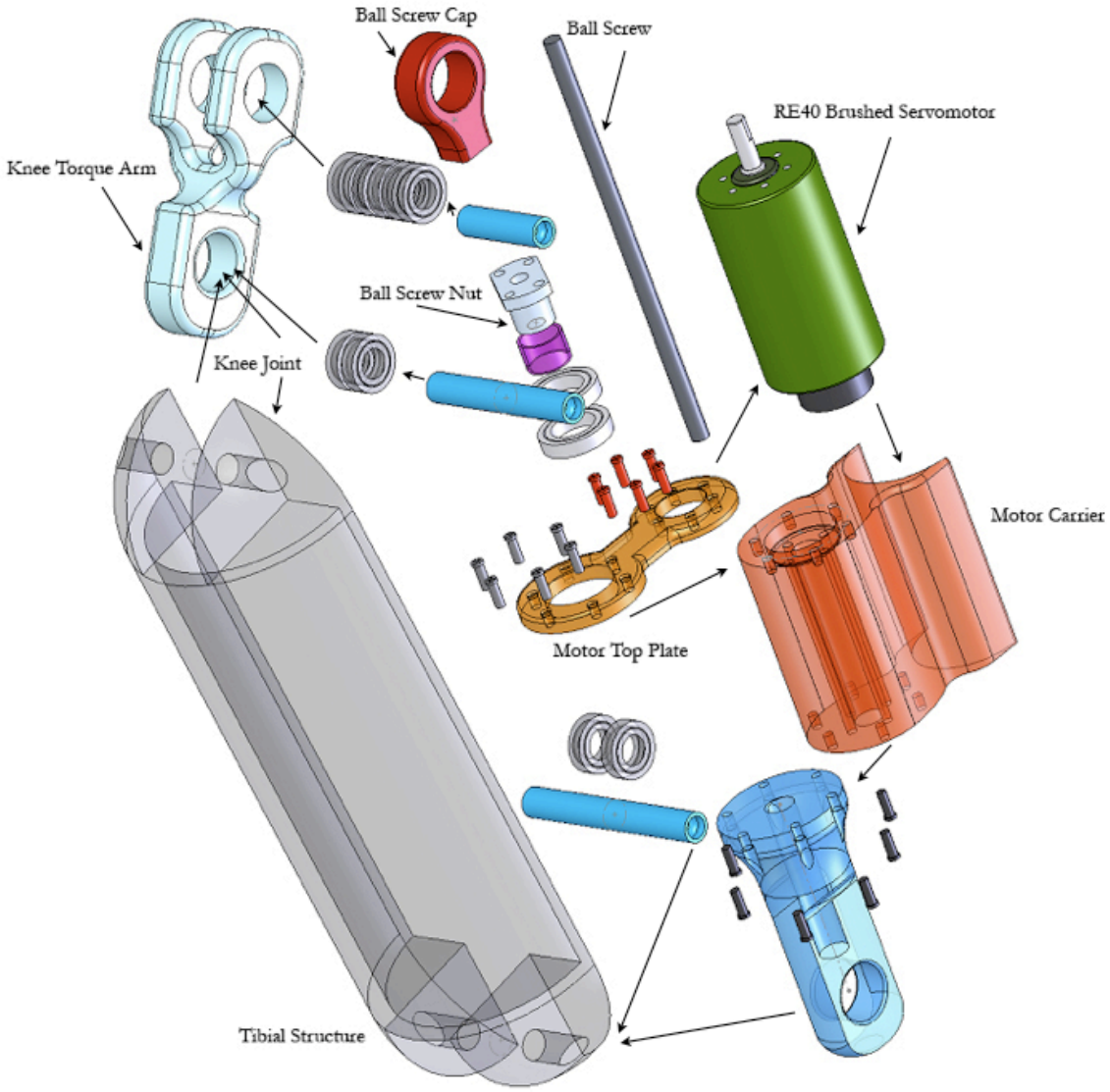

Figure 2.12: Three dimensional exploded view of the APK

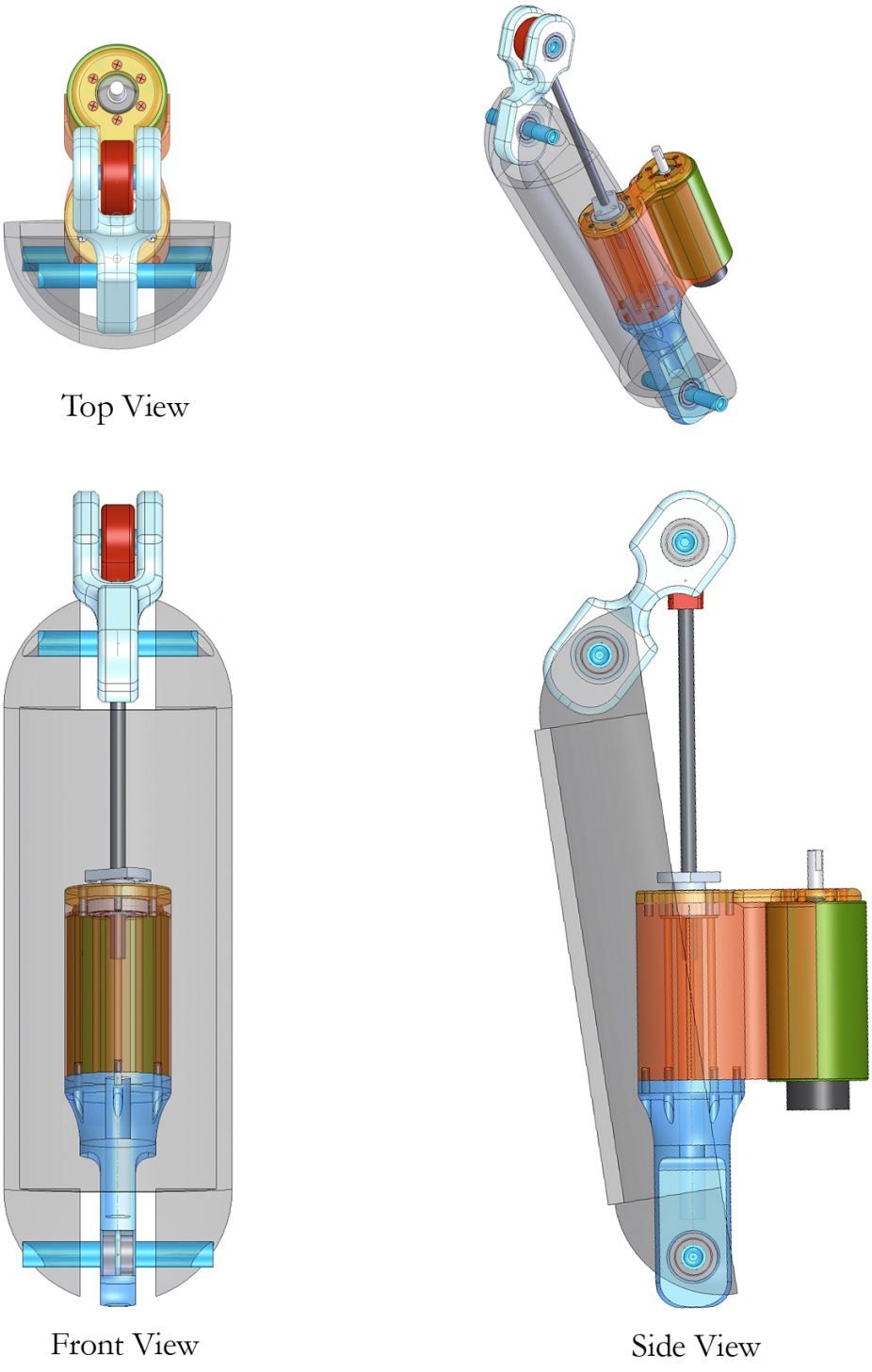

Figure 2.13: Final assembly of the APK

Figure 2.14: APK

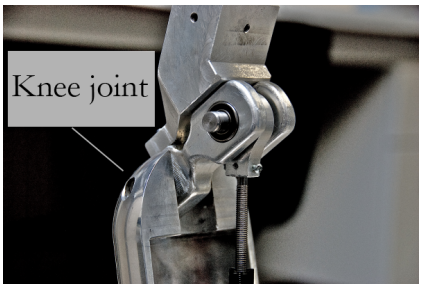

Figure 2.15: APK knee joint

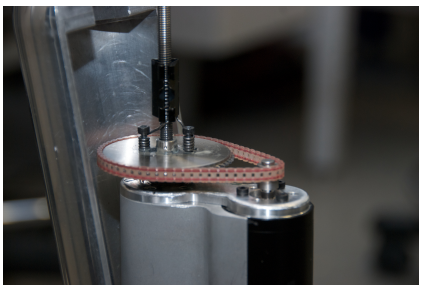

Figure 2.16: APK servomotor powered gearing

Figure 2.17: Three dimensional rendering of the APK on a person

A three dimensional simulation using SolidWorks 2006 shows a human model with the APK and its compact nature, allowing a broad demographic fit (Figure 2.17). Figure 2.18 represents the human model throughout the terminal stance onwards to pre-swing and then followed by initial swing.

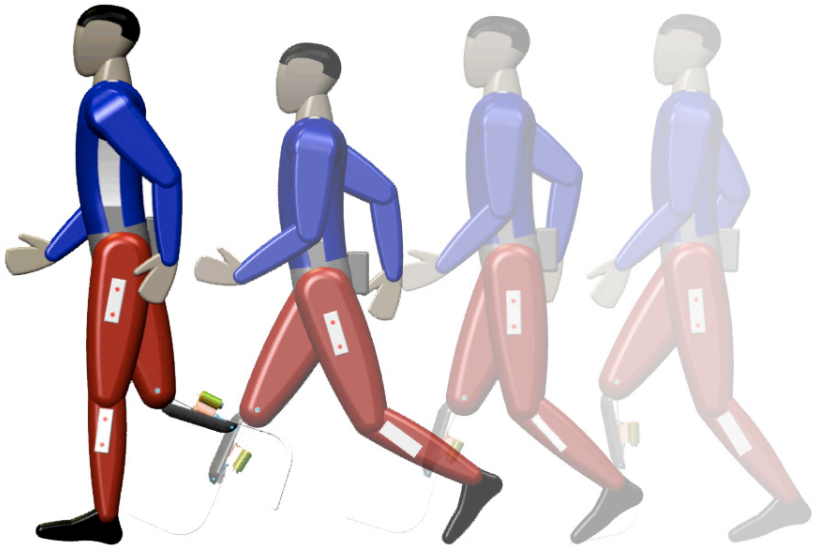

Figure 2.18: Animation of APK walking

2.3.2 Mechanical Function

The APK profile as shown in Figure 2.19, is driven by a high-speed, high-torque brushed Maxon RE40 motor, where the peak operating speed is 7,468 RPM. A gearing reduction through a precision ball-screw mechanism allows for lower operating speed. A servomotor is connected to a parallel belt-drive. A ball-screw mechanism is imbedded in the belt-pulley mechanism, where it is fixed linearly and rotates in a single axis, allowing the screw to move linearly. The linear motion of the screw, then rotates the moment arm, creating an active torque about the knee. In looking at one frame of motion, the motor rotates at 7,468 RPM with a torque of 0.201 Nm. The gear ratio of z_1 and z_2 are modular components that can be modified for optimized user comfort. In this thesis, the gearing ratio is set to 1:1. The angle α represents the adjacent angle between the screw and the moment arm. This angular velocity and acceleration can be determined taking the first and second order time derivation, respectively. The first order derivation (ω) represents the angular velocity of the knee joint. ω_m (in rev/min) represents the rotational velocity of the servomotor and ω_k (in rev/min), the rotational velocity moment arm (which essentially represents the rotation velocity of the knee joint). The lead (L), a product of the pitch and the number of starts of the ball screw, is 0.001 meters. The r is represented as the length of the moment arm between the knee joint and the connecting end of the screw, where the optimal length is 0.04 meters. The overall efficiency, η_t of the APK is estimated at a conservative 46.4%.

The angle between the axis of the torque arm (r) and the axis of the ball-screw is indicated as α, where the subscript (α_1) indicates a sample calculation. The variable $angle_1$ represents an arbitrary angle (within the range of motion) in degrees:

$$\alpha_1 = angle_1 \left[\frac{\Pi}{180} \right] \tag{1.1}$$

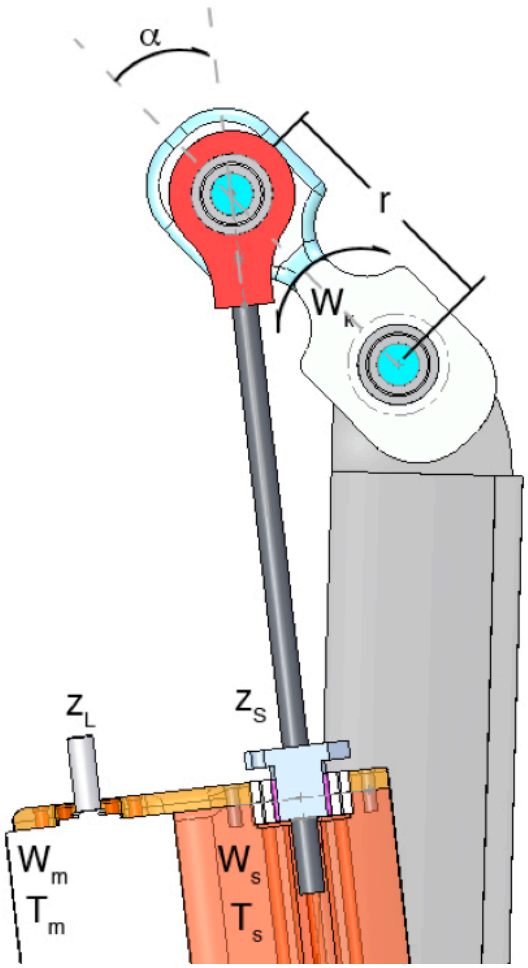

Figure 2.19: The mechanics of the APK

The required experimental rotational speed of the leg segment (knee to ankle), ω_{kr} is 0.5 rev/s (ω_k equivalent 3.142 rad/s). The required motor speed that corresponds to the experimental rotational leg speed is calculated as:

$$\omega_m = \omega_k \left[lead \left(\frac{1}{60 \cdot r \cdot \sin(\alpha_1)} \right) \cdot \left(\frac{z_1}{z_2} \right) \cdot \left(\frac{30}{\Pi} \right) \right]^{-1} \tag{1.2}$$

$$\omega_{m\text{-}rpm} = \omega_k \left[lead \left(\frac{1}{60 \cdot r \cdot \sin(\alpha_1)} \right) \cdot \left(\frac{z_1}{z_2} \right) \right]^{-1} \tag{1.3}$$

For an arbitrary angle of α_1 of 0.873 radians (50°), the required motor speed is 5,775.839 RPM (604.844 rad/s). The angle α_2 is used in the second example, where the angle is 1.57 radians (90°). Furthermore, the torque output at the knee joint T_k, is a function of the torque that is produced from the motor at its operating range.

$$T_k = T_m \cdot \left[\left(\frac{2 \cdot \Pi}{lead} \right) \cdot \left(\frac{z_1}{z_2} \right) \cdot (r) \cdot (\eta_t) \cdot (\sin(\alpha_2)) \right] \tag{1.4}$$

Figure 2.20 highlights the APK torque generation at the knee with respect to α, the angle of the knee joint.

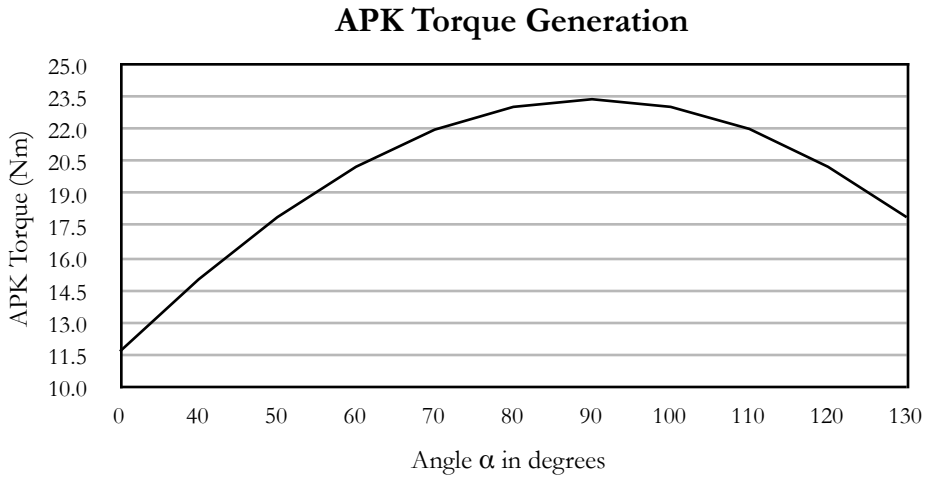

Figure 2.20: APK Knee Torque Generation versus adjacent knee angle

Based upon equations (1.3) and (1.4), the formulae for the net torque at the knee joint versus the angle α is found. The optimal settings with motor, gearing and ball-screw selection reveals that peak torque is 23.44 Nm. This corresponds to the high torque required when the subject undergoes the mid-stance and enters toe-off. The gradual build of torque can be further controlled and modulated based on torque control setting built into the microcontroller system.

2.3.3 Degrees of Freedom

The proposed APK is a simple, hinged-based device, where the knee rotation in isolation is 1-DOF. The following Gruebler's Mobility Equation for Planar Mechanisms (with Kutzbach's modification) is used to derive the system's complete DOF:

$$M = 3\,(\,n - 1\,) - 2\,f_1 - f_2 \tag{1.5}$$

where M represents the degrees of freedom of the system, n, the number of link segments, f_1 being the members with 1-DOF and f_2 with 2-DOF. The complete system is 5-DOF, where the main rotating knee joint in isolation is 1-DOF. The 1-DOF compared to the human knee of 6-DOF is greatly simplified, strictly for the purpose of greater mechanical resilience. The APK has three main anatomically equivalent components: the upper tibia, knee joint and the moment arm that creates the active torque for the knee joint.

2.3.4 Servomotor Integration

The servomotor used is a Maxon RE40 graphite brushless motor (refer Appendix A). The RE40 is capable of running at a peak operating torque of 0.201 Nm at an operable speed of 8,200 RPM. The motor measures 40 mm in outer diameter and total length (including shaft) is 91.3 mm. The RE40 was chosen as the motor due to its small size, weight, resulting in minimal rotational inertia when operating at higher rotational speeds.

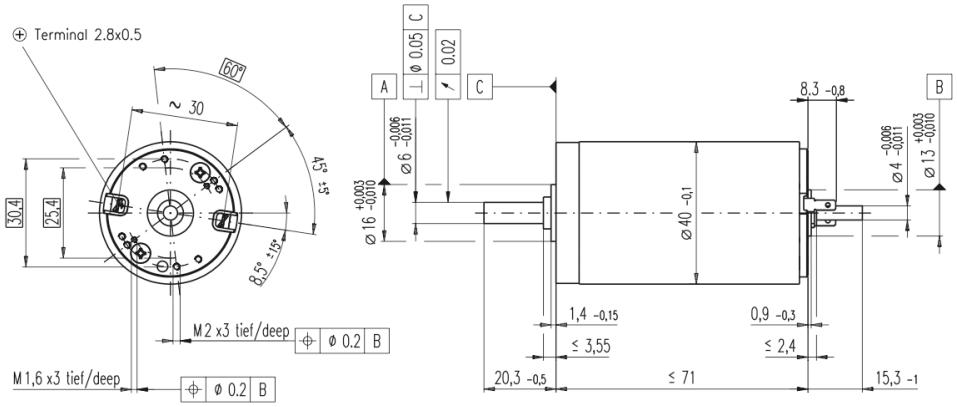

Figure 2.21: Maxon RE40 Graphite Servomotor (Maxon, 2005)

The motor's remotely powered operation is not considered in this research. Figure 2.22 highlights the portion in red, which is the recommended operating range of the motor.

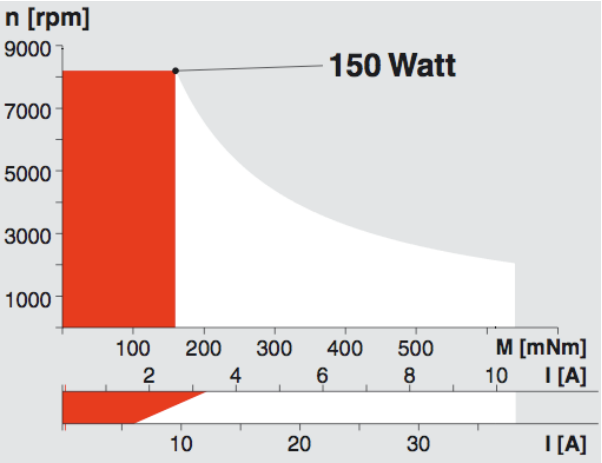

Figure 2.22: Maxon RE40 Program Operating Range

Table 2.2: Maxon RE40 Specification Table (Maxon, 2005)

Power Rating	150 W
Nominal Voltage	48 V
No Load Speed	7580 RPM
Stall Torque	2.5 Nm
Torque Constant	60.3 nMm/A
Speed Constant	158 RPM/V
Max. Permissible Speed	8,200 RPM
Max Continuous Torque	0.201 Nm

2.3.5 Electromagnetic Field Effects

In analyzing Figure 2.23, it is found that the motor is situated approximately 10-15 cm distal to the femur (varies with the severity of the amputation and socket length). Further, as the servo will be turned on for extended periods of time, the study is to determine the electromagnetic field (EMF) intensity that is emitted by the Maxon RE40 brushed servo motor. The experiment was conducted by placing the LakeShore Model 410 Gauss meter at various distances from the motor. This was then corresponded and compared with the the study by Yousef Haik et. al. (2001) and determined whether or not the EMF emitted by the RE40 is in anyway harmful to the user.

Figure 2.23: The APK's close proximity to the biological system

The experiment was conducted in such a way that it was operating at 75% of full running capacity at approximately 6,000 RPM. Using the LakeShore Model 410 and a high precision robot, the gauss meter was attached to the automated robot arm, whereby a controlled 5 mm interval was determined to run from the top to the bottom of the motor. The motor was situated on an EMF-free table in isolation. The LakeShore 410 was then passed in the Y-axis at 5 mm intervals. Further, each reading was determined final when it reached steady state.

The first placement was the LakeShore 410 being 2 mm from the motor (Figure 2.24). The peak intensity was found to be -1.21 mT, where the top portion of the motor represented the

negative pole, whilst the bottom portion near the encoder peaked at +0.24 mT. However, for all tests, it was found that although the peak intensity was identified at exactly the midpoint of the motor, the negative pole continued slightly below the center point and the negative intensity as a whole read higher amplitudes than that of the positive pole. This is likely due to the fact that the motor's top portion contains the fastening bracket.

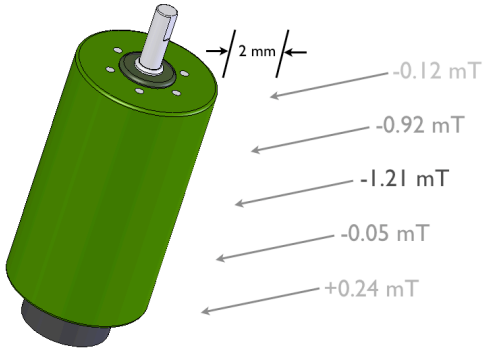

Figure 2.24: EMF at 2 mm

The second distance was placed at 8 mm away from the running motor, as shown in Figure 2.25. At four times the first distance, the field intensity correspondingly decreased as well, by nearly 2.4 times. The peak value was found to be -0.5 mT.

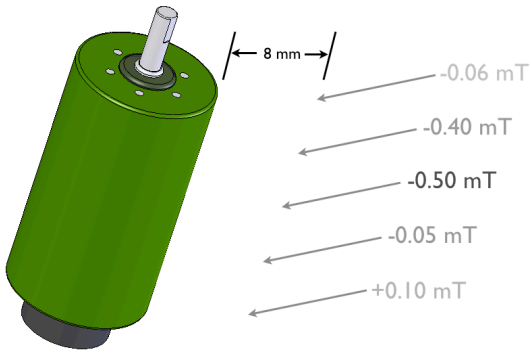

Figure 2.25: EMF at 8 mm

As the distance was then spread further to 15 mm (Figure 2.26), the peak intensity was found to be -0.29 mT, linearly corresponding with the 8 mm to 15 mm distance by dropping in half.

The signs of a greater negative pole was still apparent and was unique to the characteristics of the motor.

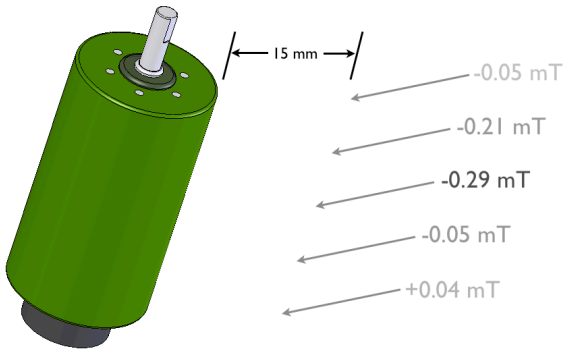

Figure 2.26: EMF at 15 mm

Lastly, as the motor was pulled away to 35 mm (Figure 2.27) and further, the reading dropped and approached 0 mT. Hence it was determined that there would in fact be no interference with the transfemoral stump.

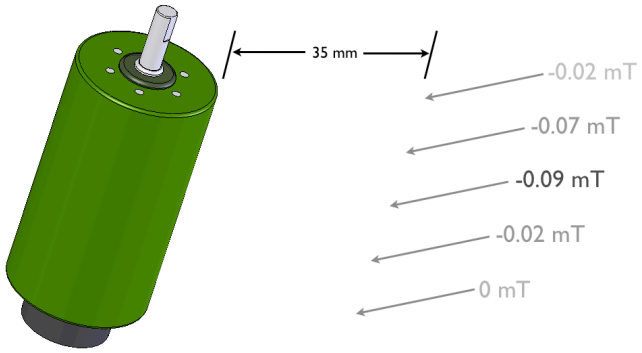

Figure 2.27: EMF at 35 mm

Furthermore to reinforce the fact that there were no EMFs, the gauss meter was pulled 35 mm from the motor. It was determined through this test, that the motor is adequately shielded from EMF interference.

Chapter 3

Finite Element Analysis

3.1 Introduction

The APK was entirely modeled in the three dimensional computer aided engineering program SolidWorks 2006. Once the modeling was complete, the assembly files were exported into a finite element analysis (FEA) program ANSYS Workbench (WB) 11, where the physical system was modeled based on gait data. FEA is a numerical and mathematical interpretation of a physical system, and in the case of the APK study, investigated the stresses and deformations once it was loaded in the cyclical gait cycles for real human data. The FEA process looks into three major components: pre-processing, analysis and post-processing. The pre-processing component looks into setting the problem, by having the APK replicate the motions of a healthy leg. Boundary conditions `and criteria is set to define the physical model of the APK. The system is then meshed, using three dimensional tetrahedral elements. The second step looks into the analysis of the model, and allows for a visual representation of the stresses and deformations acting. Lastly, the post-processing aspect looks into the cyclical load characteristics as well as the minimum and maximum values of the stress analysis.

3.2 Solid Modeling

The entire APK was modeled using SolidWorks. There were thirteen structural components which were designed, twelve ball bearings and eighteen screws and bolts, as shown in Figure 3.1. Once each part was designed, it was given its respective material property. All the unique components were then assembled in SolidWorks and the pre-made purchased component part files were imported directly from the manufacturer's sources. As the prototype was to be built in 6061 aluminum, the model was also assigned the same material, accordingly. Purchased component material properties were assigned from the factory.

Once the entire model was complete, the total mass of the APK in the SolidWorks was calculated to be 1.63 kg. The SolidWorks assembly was then exported into a Parasolid model, for importing into ANSYS.

3.3 Pre-Processing

3.3.1 Model Simplification

The original APK model complexity was reduced to a simpler model as smaller components only required greater computing resources with nearly identical results. Minor components such as screws, bolts and bearings were simplified as extensions of the larger structural member as bonded joints. Press fittings and Loctite® links were also simplified as bonded surfaces. The overall purpose of the FEA study is to examine closely the effects of the main structural components and its mechanical resilience through heavy cyclical loading.

Figure 3.1 shows the original rendering versus the simplified model rendering. The simplification resulted in a more accurate result for the FEA study. The original APK assembly of 43 unique parts were collaborated to make six unique parts. Each simplified link was closely examined so that results would maintain accuracy. The model components *arm, tibia, cap* and *structure* are 6061 aluminum, while the *screw* and *servo* are structural steel (as shown in Figure 3.2).

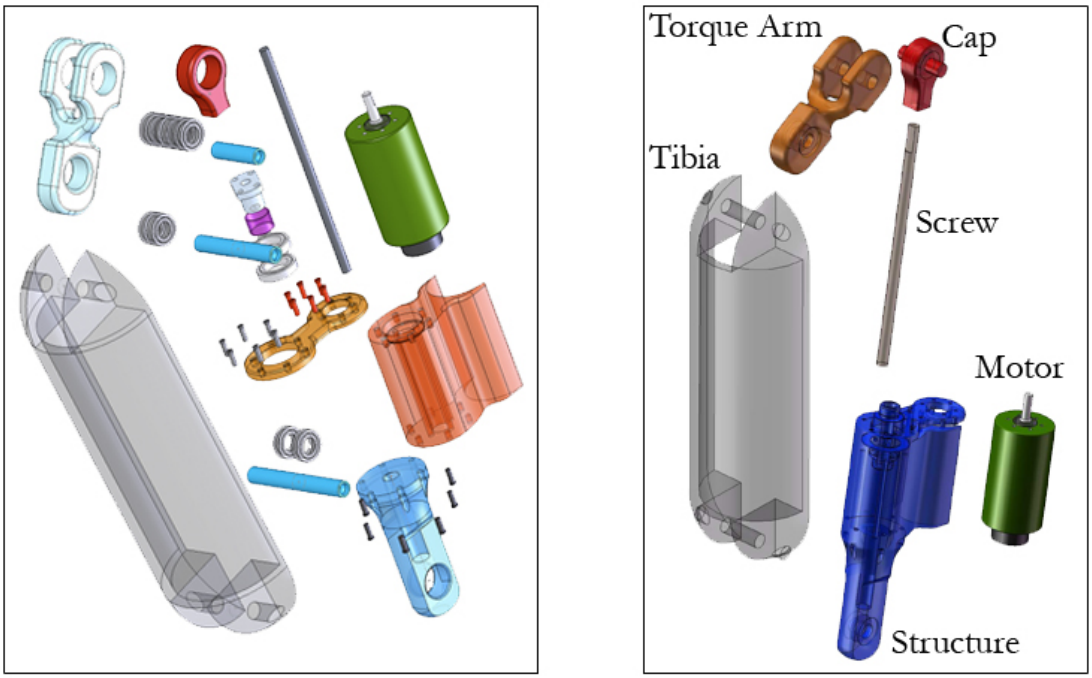

Figure 3.1: Comparison of the full assembly (left) and simplified assembly (right)

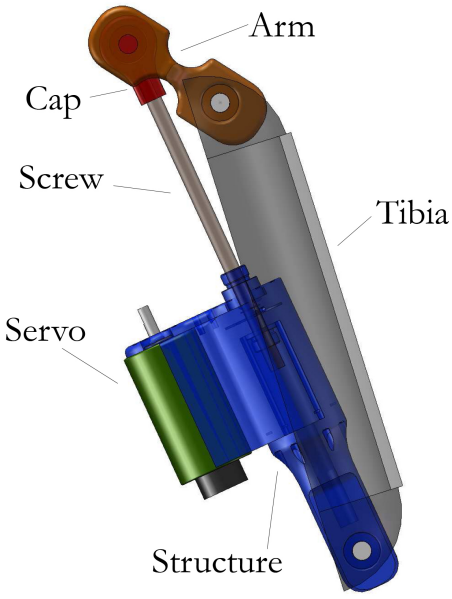

Figure 3.2: Simplified model

3.3.2 Gait Modeling

The human gait model for the FEA study is based on actual recorded data from the University of Waterloo Kinesiology Department (Winter, 2005). The trial was based on a male subject with a mass of 56.7 kg and leg length (lateral epicondyle to lateral malleolus) of 42.5 cm. Furthermore, the data sampling rate frequency is based on 69.9 frames per second (FPS) from force sensors. Electrodes and force sensors attached to each limb allowed precise measurements of loads and dynamic movements that are exerted at the joints. The data for the lateral epicondyle (knee) and lateral malleolus (ankle) was used to model the system.

The entire gait cycle was not used in the FEA study, as the swing phase loads were negligible. Based on Figure 3.3, the portions of when the leg in stance phase was used, as the loads were most significant during these phases. The coordinates, knee angles, force vectors and moments were used. Since the APK measures 1.63 kg (approximately 2 kg with a tibial extension with foot) and the anatomical leg at 2.4 kg, the forces are assumed to be equal.

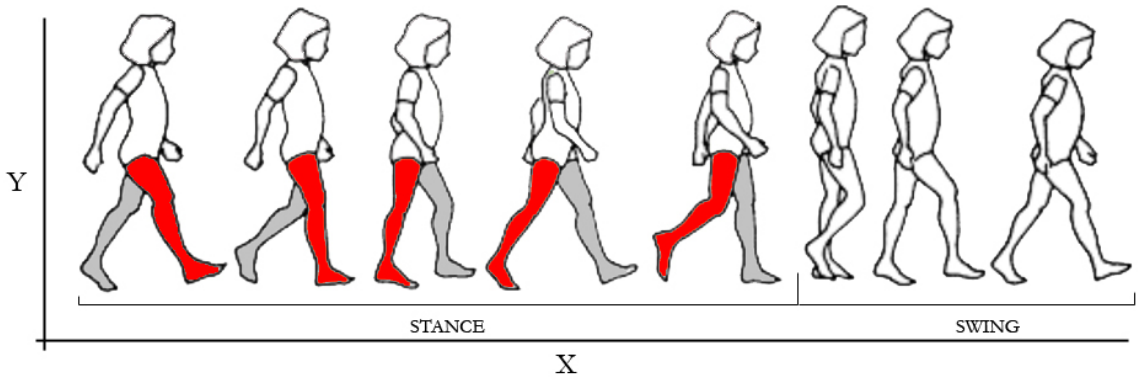

Figure 3.3: The stance portion of the gait cycle

Based on the Winter study (2005), 106 frames were captured, where the sampling rate is 69.9 FPS, totaling 1.51 seconds of total capture. Based on the data, frames 28 to 68 comprised the stance phase and therefore data from these frames were used. The APK FEA model was analyzed frame by frame. However, instead of capturing and conducting studies on all frames from 28 to 68 inclusive, all even numbered frames were used. Hence, 21 frames in total. Each

frame was studied individually, analyzing in great details the loaded characteristics of the APK. Each frame also provides the coordinates of the joints as well as the load and moments. The net angle of the femur to tibia was calculated based on geometry of the coordinate system. The forces in the X-direction are found to be small in comparison to the Y-direction loads in compression due to the torso weight and the corresponding ground reaction force, as shown in Figure 3.3. The largest compressive force occurs at frame 17, which is approximately 81% of the stance phase. This portion correlates to the terminal stance phase, where only one leg bears all the upper body load. Table 3.1 presents each of the 21 unique frames and the instantaneous loads applied at that given moment at the knee and ankle joints. Each force and moment is applied to the corresponding joints on the APK. The minimal loads occur when the subject steps into heel contact at the beginning of the gait cycle.

Table 3.1: Stance phase forces and moments

Frame	**Knee Force X (N)**	**Knee Force Y (N)**	**Knee Moment (N!m)**	**Ankle Force X (N)**	**Ankle Force Y (N)**	**Ankle Moment (N!m)**
1	-64.3	-50.2	-33.8	48.7	82.4	1.7
2	27.2	-255.2	-7.6	-38.2	292.9	-8.3
3	77.7	-429.9	7.8	-88.4	463.4	-6.9
4	91.5	-516.7	24.8	-108.1	541.1	-5.0
5	91.7	-568.4	35.0	-109.4	589.9	0.5
6	63.7	-558.2	32.5	-78.5	581.7	3.5
7	36.8	-481.5	24.8	-47.2	508.7	6.6
8	29.8	-395.6	19.8	-32.7	425.2	10.6
9	24.6	-344.7	10.9	-22.4	369.4	18.7
10	21.0	-333.8	6.6	-17.4	355.0	25.3
11	20.7	-343.7	7.0	-17.5	367.3	30.3
12	13.0	-364.3	2.3	-10.3	392.4	38.8
13	-0.9	-402.2	-0.1	2.1	432.7	45.4
14	-12.3	-453.7	-6.2	16.8	484.4	58.8
15	-30.9	-513.0	-10.4	40.4	542.9	71.2
16	-53.3	-559.3	-12.4	67.7	586.9	82.7
17	-63.1	-576.4	-6.4	87.4	602.8	89.7
18	-68.9	-538.7	2.3	103.8	565.0	86.7
19	-67.5	-421.9	10.1	105.7	450.2	68.6
20	-46.1	-240.4	13.3	77.2	269.9	38.8
21	-4.1	-71.2	10.6	26.7	101.8	12.3

3.3.3 Meshing

The meshing component (Figure 3.4) is based on round non-straight sided tetrahedral elements in triangular formation, with three nodes per element. The element sizes are based on default settings in ANSYS, and the physics preferences are based on the mechanically optimized mesh setting. On average, each FEA frame resulted in approximately 100,000 nodes and 55,000 elements.

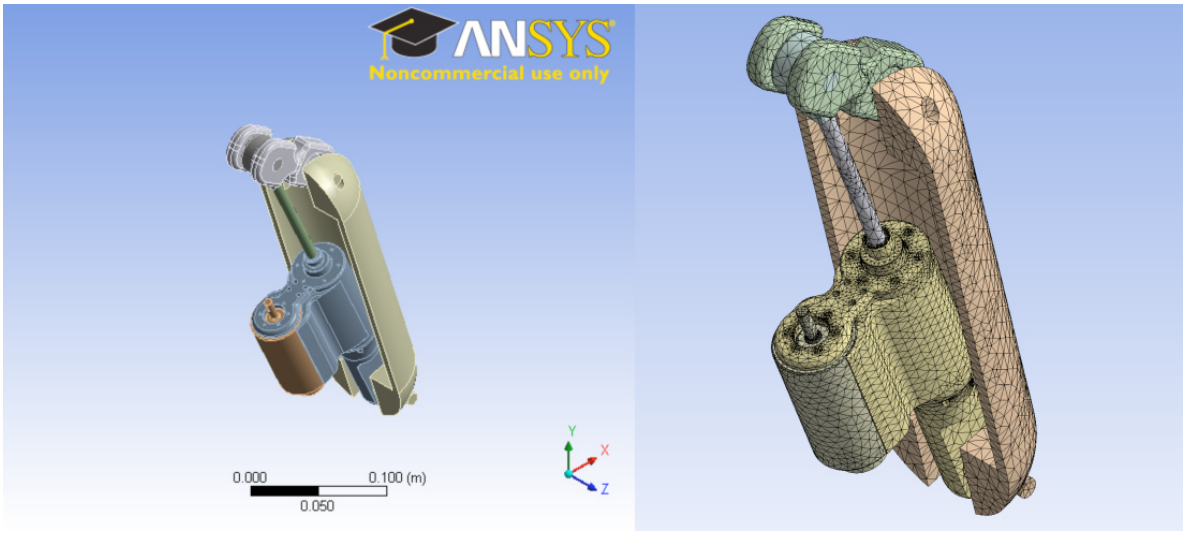

Figure 3.4: Isometric view (left) and mesh view (right)

3.3.4 Boundary Conditions and External Reactions

The APK model designed in SolidWork was processed as a Parasolid file form and then imported into ANSYS Workbench. Each of the assembly mates had to be re-modified in ANSYS, as some of the contact surfaces were modified throughout the file changing process. One primary boundary condition was to pin down the lower end distal to the knee joint, shown in Figure 3.5. There are two compressive forces and two moments at the knee joint and the distal end, as shown in Figures 3.6 and 3.7.

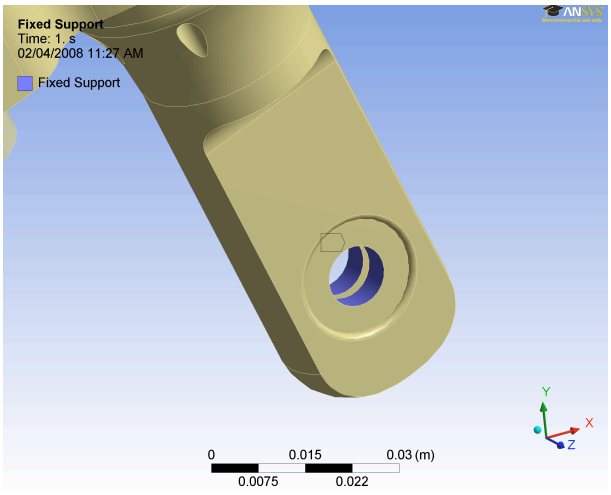

Figure 3.5: Fixed boundary condition

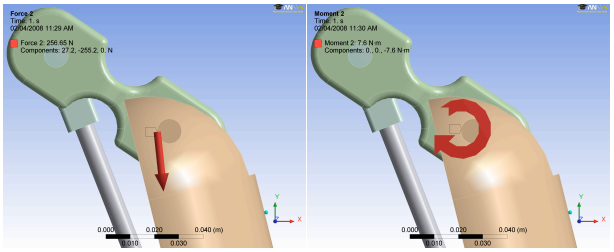

Figure 3.6: Force component in X-Y axes and moment about the Z axis at the knee joint

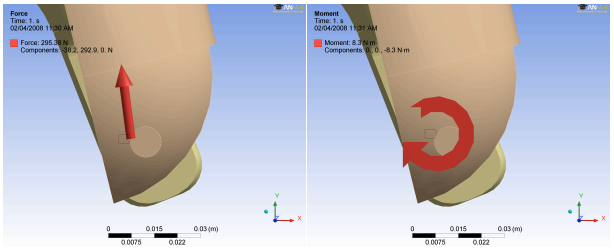

Figure 3.7: Force component in X-Y axes and moment about the Z axis at the ankle

3.4 Analysis

Upon placing compressive loads and joint moments, various stress and strain analyses are investigated. The equivalent stress analysis reveals the triaxial compressive forces that act upon the overall system. The shear stress looks at the forces that are acting in parallel against facing surfaces. The equivalent von-Mises strain analysis involves the deformation and the total deformation study involves the maximum and minimum components that deform. All the FEA study results are found in Pascals and strains in meters per meter (m/m). Figures 3.8 to 3.12 shows the mesh and four simulations, respectively.

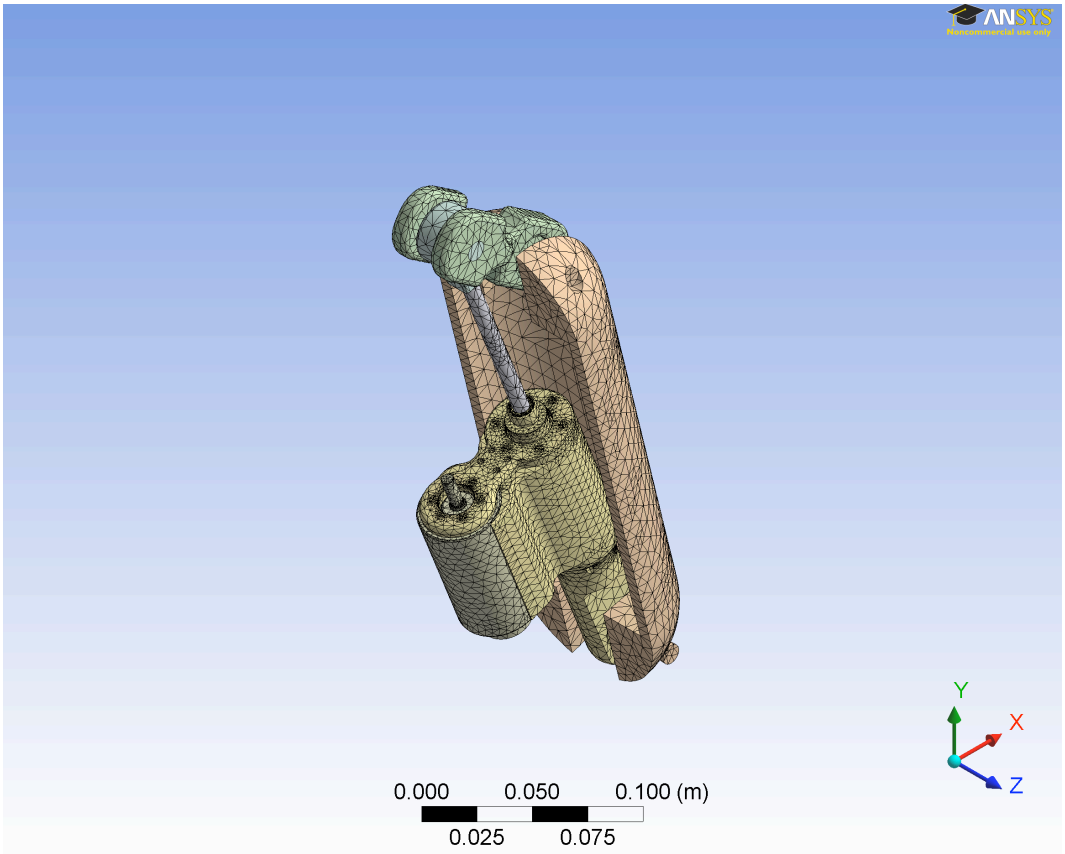

Figure 3.8: Pre-analysis mesh

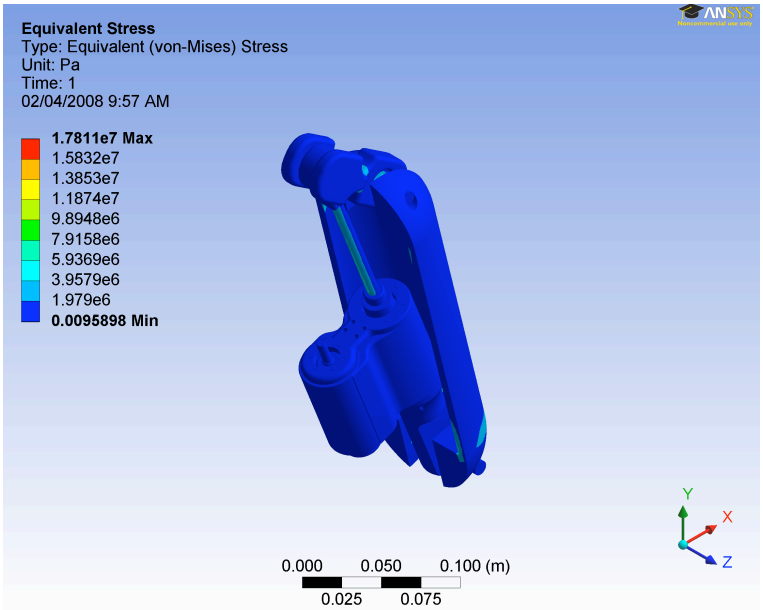

Figure 3.9: Equivalent (von-Mises) stress analysis

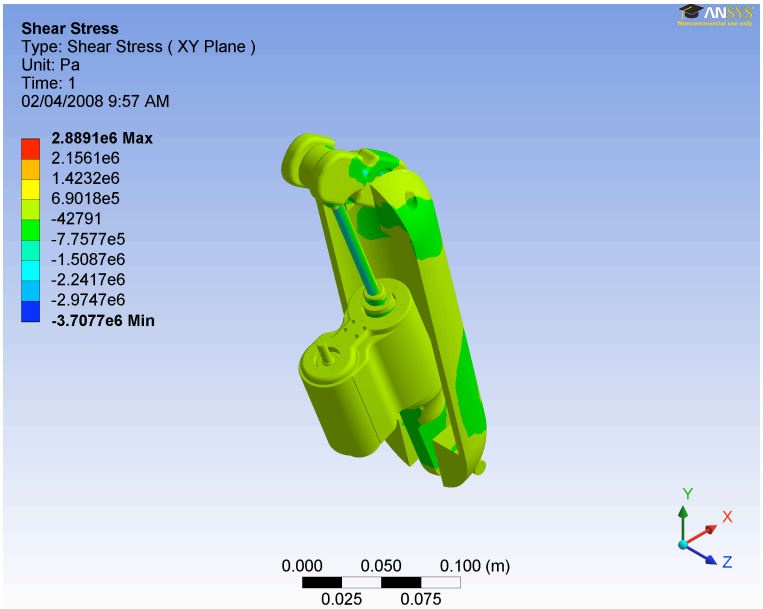

Figure 3.10: Shear stress analysis

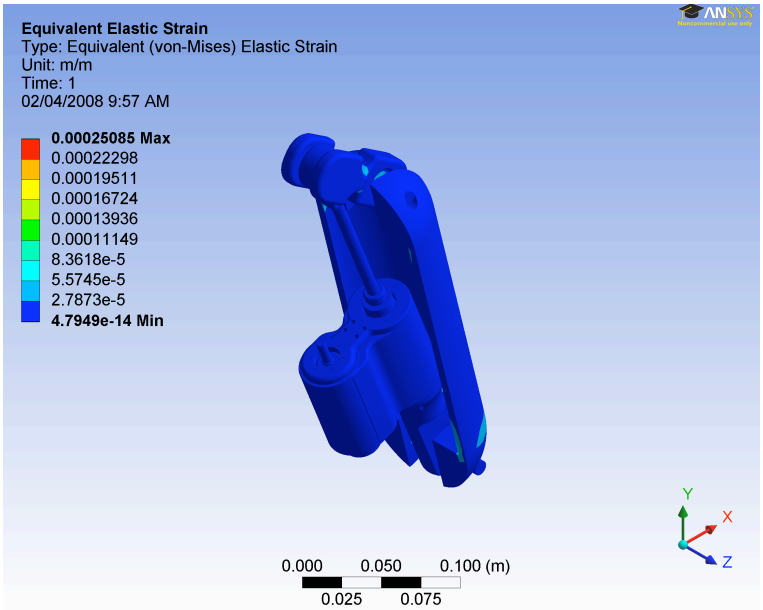

Figure 3.11: Equivalent (von-Mises) strain analysis

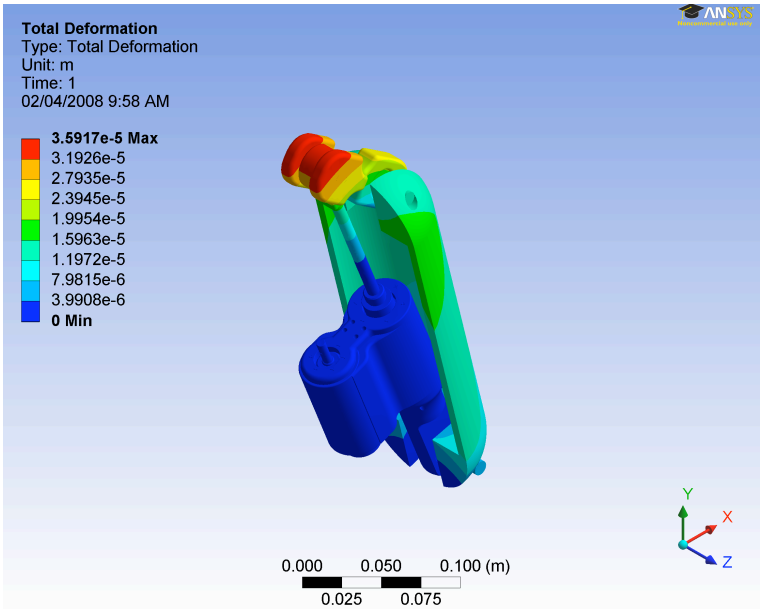

Figure 3.12: Total deformation analysis

3.5 Post-Processing

3.5.1 Equivalent (von-Mises) Stress Analysis

The triaxial loading analysis reveals that the weakest component is the ball screw joint. This is due to the fact that the ball screw is the thinnest point of the APK structure. At the peak loading point, the maximum stress climaxes at 107.91 MPa at the terminal stance phase. The lowest point of loading occurs consistently at the RE40 servomotor (as shown in Table 3.2), where no stresses are noted.

Table 3.2: Equivalent (von-Mises) stress analysis

Frame	Max stress (MPa)	Location	Min stress (MPa)	Location
1	56.65	Screw	0	Servo
2	17.81	Tibia	0	Servo
3	29.59	Screw	0	Servo
4	52.25	Screw	0	Servo
5	63.04	Screw	0	Servo
6	68.75	Screw	0	Servo
7	40.96	Screw	0	Servo
8	26.47	Screw	0	Servo
9	14.36	Arm	0	Servo
10	18.7	Screw	0	Servo
11	22.23	Screw	0	Servo
12	34.35	Screw	0	Servo
13	45.08	Screw	0	Servo
14	71.76	Screw	0	Servo
15	89.14	Screw	0	Servo
16	107.91	Screw	0	Servo
17	106.91	Screw	0	Servo
18	94.43	Servo	0	Servo
19	63.15	Screw	0	Servo
20	35.93	Tibia	0	Servo
21	12.66	Tibia	0	Servo

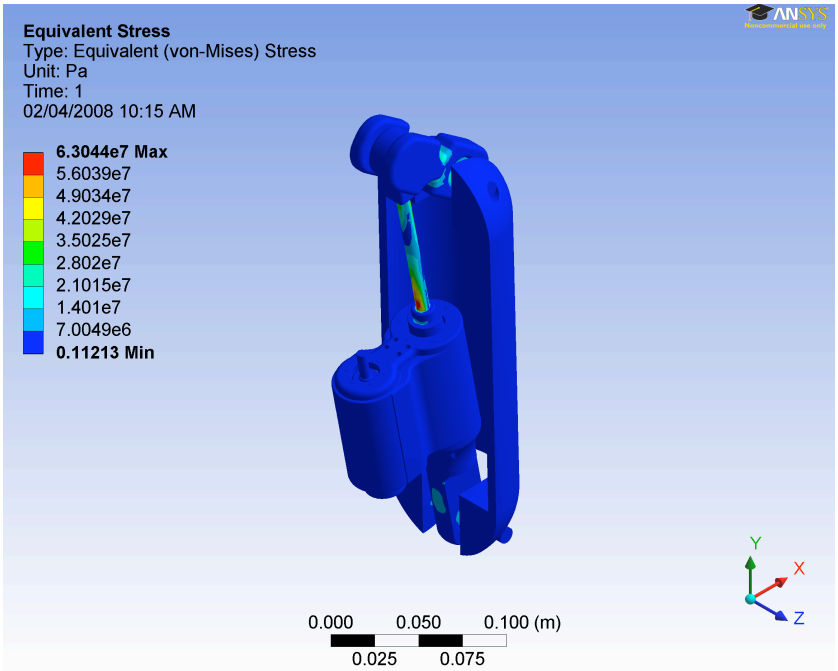

Figure 3.13: Equivalent stress for Frame 5 (initial contact)

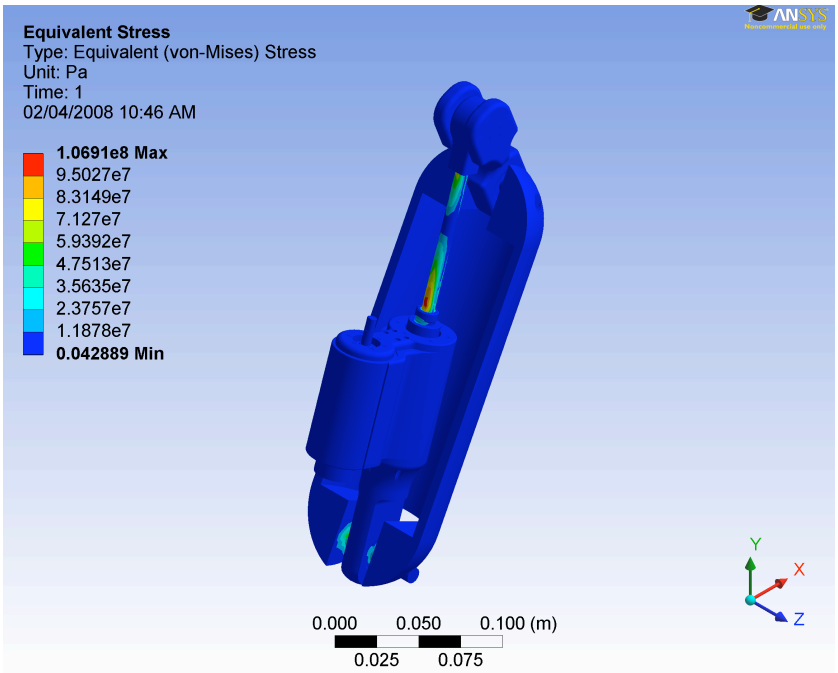

Figure 3.14: Equivalent stress for Frame 17 (terminal stance)

3.5.2 Shear Stress Analysis

The shear stress components are found to correspond to the equivalent stress analysis, where both the maximum and minimum shear occur at various structural components. As the gait cycle progresses from heel contact, the ball screw and structural components undergo maximum and minimum stresses respectively. As the subject approaches the mid-stance phase, the main structure experiences the greatest shear stress. The greatest shear stress is subjected on the structure at 35.37 MPa in frame 17 (Table 3.3).

Table 3.3: Shear stress analysis

Frame	Max shear (MPa)	Location	Min shear (MPa)	Location
1	15.89	Structure	-20.8	Screw
2	2.89	Arm	-3.71	Tibia
3	8.53	Screw	-8.39	Structure
4	12.25	Screw	-14.63	Structure
5	18.57	Servo	-21.19	Structure
6	18.32	Servo	-15.1	Arm
7	11.31	Arm	-11.88	Structure
8	7.34	Arm	-9.66	Arm
9	5.75	Tibia	-5.99	Arm
10	8.49	Structure	-4.89	Arm
11	8.04	Structure	-4.78	Arm
12	10.02	Structure	-11.8	Servo
13	12.89	Structure	-11.19	Servo
14	16.25	Structure	-10.13	Tibia
15	24.81	Structure	-16.5	Tibia
16	27.24	Screw	-28.09	Servo
17	35.37	Structure	-31.68	Screw
18	31.34	Screw	-32.87	Screw
19	25.55	Screw	-24.28	Screw
20	10.39	Screw	-12.94	Screw
21	3.89	Arm	-5.17	Arm

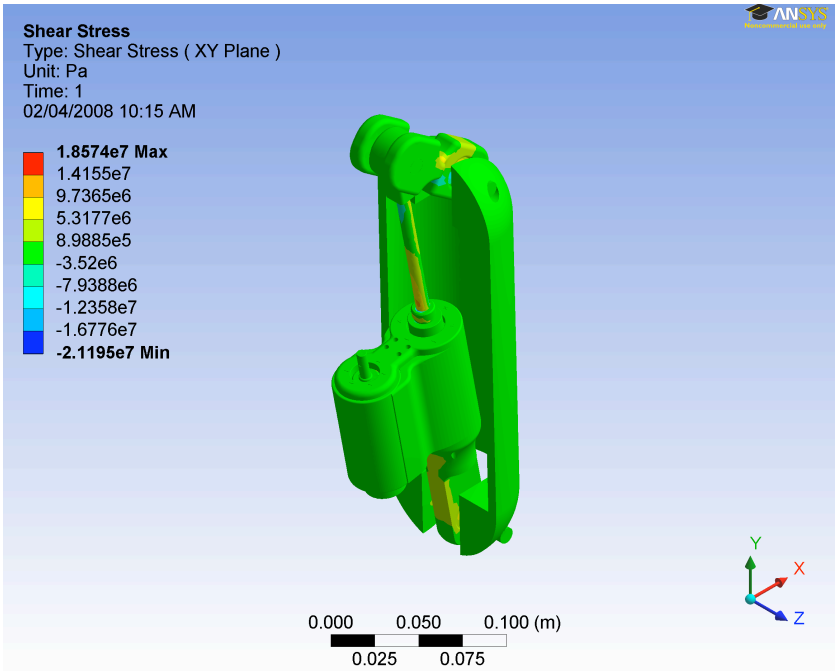

Figure 3.15: Shear stress for Frame 5 (initial contact)

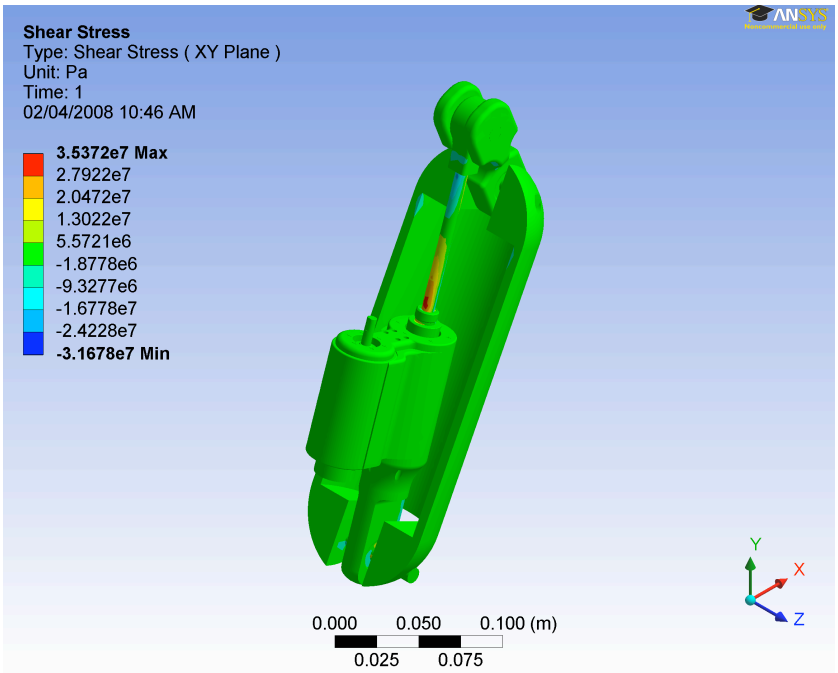

Figure 3.16: Shear stress for Frame 17 (terminal stance)

3.5.3 Equivalent (von-Mises) Strain Analysis

Much like the equivalent (von-Mises) stress analysis, the stain component corresponds, in that the servomotor undergoes the least strain. Throughout the initial heel strike, the arm undergoes the greatest strain. This is likely due to larger knee angle. However, as the subject undergoes terminal stance, the tibia experiences the largest strains as shown in Table 3.4, frame 17.

Table 3.4: Equivalent (von-Mises) strain analysis

Frame	Max strain (m/m)	Location	Min strain (m/m)	Location
1	0.000678	Tibia	0	Servo
2	0.00025085	Tibia	0	Servo
3	0.00022508	Structure	0	Servo
4	0.000459	Structure	0	Servo
5	0.00058	Arm	0	Servo
6	0.000511	Arm	0	Servo
7	0.000379	Arm	0	Servo
8	0.000319	Arm	0	Servo
9	0.000202	Arm	0	Servo
10	0.000253	Structure	0	Servo
11	0.000227	Tibia	0	Servo
12	0.00033	Tibia	0	Servo
13	0.000369	Tibia	0	Servo
14	0.000551	Tibia	0	Servo
15	0.000762	Tibia	0	Servo
16	0.000856	Structure	0	Servo
17	0.00109	Structure	0	Servo
18	0.000812	Tibia	0	Servo
19	0.000584	Structure	0	Servo
20	0.000506	Tibia	0	Servo
21	0.000178	Tibia	0	Servo

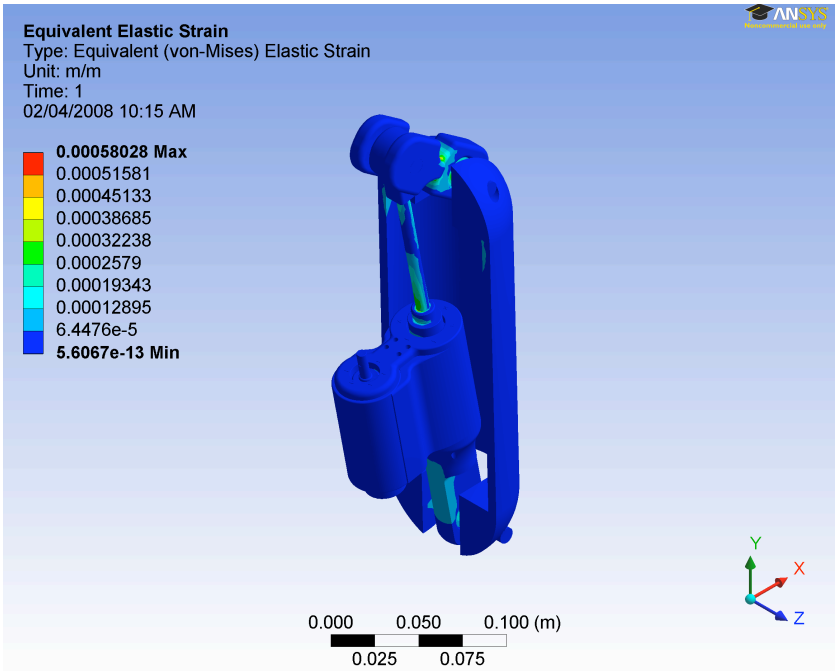

Figure 3.17: Equivalent strain for Frame 5 (initial contact)

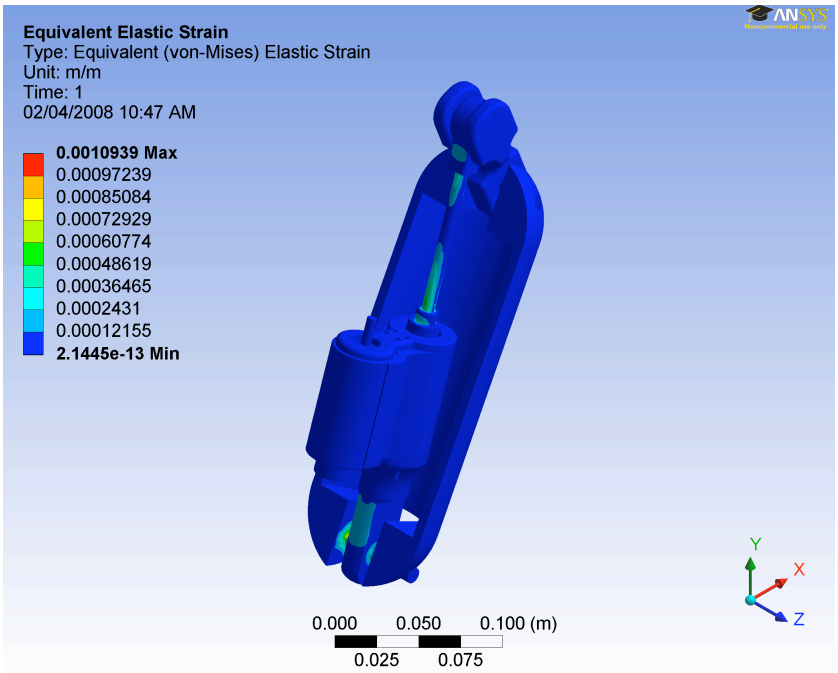

Figure 3.18: Equivalent strain for Frame 17 (terminal stance)

3.5.4 Total Deformation Analysis

The greatest deformation is sustained on the arm throughout most of the stance phase. The weight saving aspects is the cause of the large deformation of 0.659 mm (Table 3.5, frame 16), a significant amount which hinges into the plastic deformation. As such, a redesign of the arm component would resort to foregoing the weight saving portion and a more substantial design would be required. The structure undergoes the least deformation and is seemingly unaffected. The further reinforcing will further promote structural integrity and long lasting viability.

Table 3.5: Total deformation analysis

Frame	Max def'm (mm)	Location	Min def'm (mm)	Location
1	0.3	Arm	0	Structure
2	0.0359	Arm	0	Structure
3	0.1253	Screw	0	Structure
4	0.234	Arm	0	Structure
5	0.266	Arm	0	Structure
6	0.257	Arm	0	Structure
7	0.165	Screw	0	Structure
8	0.0815	Arm	0	Structure
9	0.0347	Arm	0	Structure
10	0.116	Arm	0	Structure
11	0.142	Arm	0	Structure
12	0.226	Arm	0	Structure
13	0.286	Arm	0	Structure
14	0.427	Arm	0	Structure
15	0.557	Arm	0	Structure
16	0.659	Arm	0	Structure
17	0.657	Arm	0	Structure
18	0.564	Arm	0	Structure
19	0.366	Arm	0	Structure
20	0.148	Arm	0	Structure
21	0.01607	Arm	0	Structure

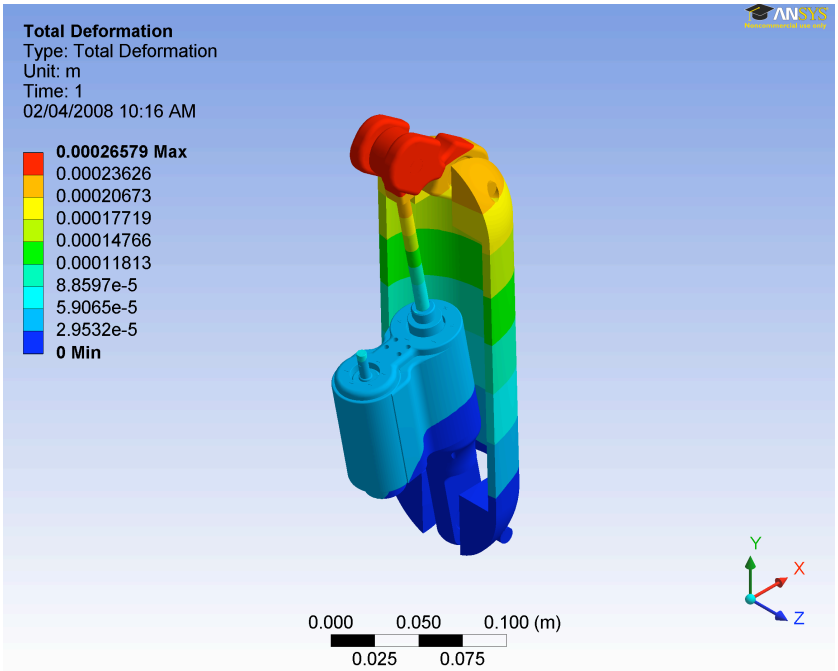

Figure 3.19: Total deformation for Frame 5 (initial contact)

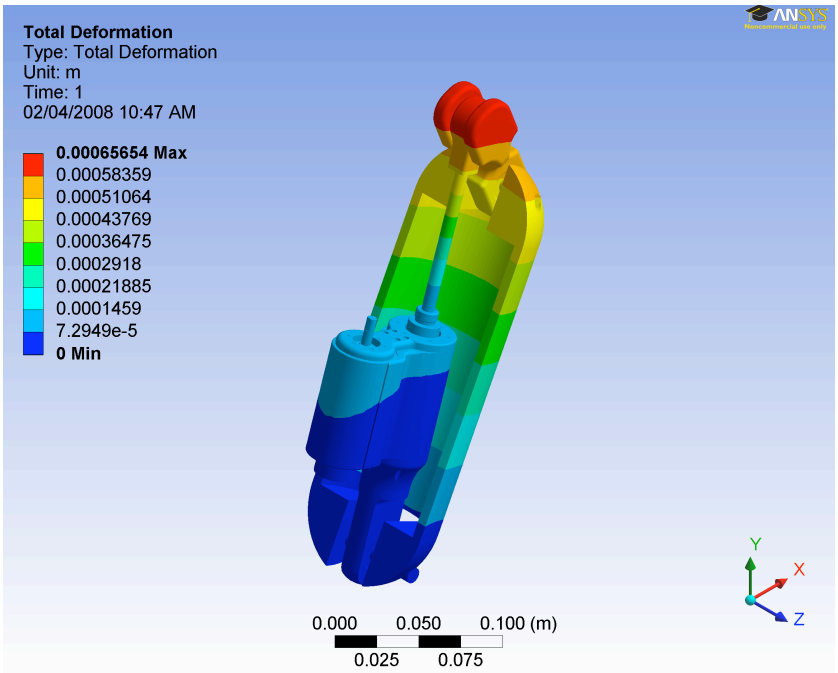

Figure 3.20: Total deformation for Frame 17 (terminal stance)

3.5.5 Cyclical Loading

The cyclical loading versus the number of cycles for aluminum applies to all of the components with the exception of the ball screw and the servomotor. In looking at the equivalent stress, the maximum value of 107.91 MPa corresponds to approximately 1.6 million cycles. Furthermore, the peak equivalent stress experienced by the ball screw (made of steel), has a much lower cyclical life, that under maximum loading, it can undergo approximately 20,000 cycles. The stress versus cycles results are based on the analysis provided by the ANSYS FEA study.

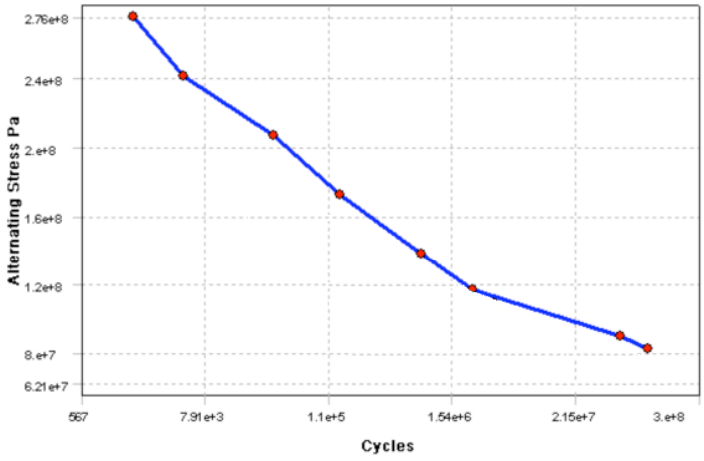

Figure 3.21: Alternating stress versus cycles (S-N Curve) for aluminum

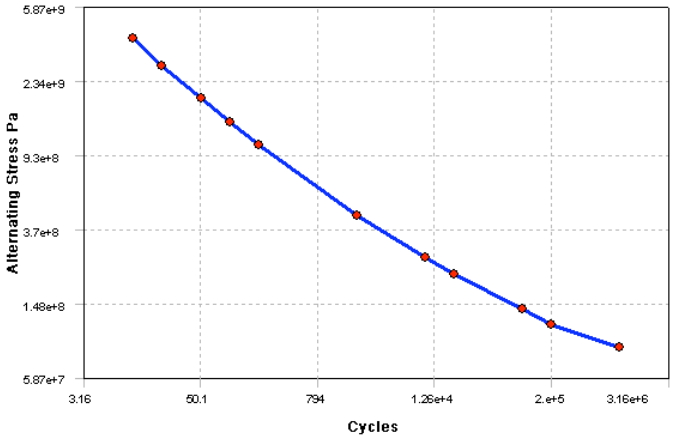

Figure 3.22: Alternating stress versus cycles (S-N Curve) for steel

3.6 Discussion

Finite element analysis in general, provides a visual and mathematical interpretation of a physical system. The APK model is simplified from the original model, as 21 unique motion frames. Unnecessary model complexities result in longer calculating times and a greater margin of error. Minor parts were conjoined to its parent structural component. Hence, some of the smaller components were simplified by aggregation to larger structures.

The FEA followed three steps: pre-processing, analysis and post-processing. The results presented mathematical models to visualize and predict alternating stresses for cyclical loads. The analysis investigates four simulations: 1) equivalent stress, 2) equivalent strain, 3) shear stress and 4) total deformation. Although the FEA study is not a perfect model, it presents and highlights much of the short comings and limitations of the APK design. It is found that the greatest loads generally occur at frames 15-17, where the subject undergoes mid-stance onwards to terminal stance, where the greatest load is borne by the knee joint. As expected, the servomotor is unaffected by any of the loads, with its placement in isolation. The ball screw system and the structural components had the greatest effects as they are the primary load bearing components. The weight saving designs are found not to be beneficial, but more of a structural compromise. A significantly robust redesign will allow for increased lifespan and structural integrity.

Chapter 4

Controller Design

4.1 Control Design Integration

The motivation of the controls for the APK is to send a correct value of torque to the actuator of the APK associated with the angular position of the tibia and femur of the healthy leg. As shown in Figure 4.1, an encoder feedback can be utilized to compare the desired position of the APK with the real position based on the Winter data (2005) for knee angle versus percentage of the gait cycle (refer Figure 2.7). The position error will be sent to a proportional–integral–derivative (PID) controller to adjust the real position of the APK. Figures 4.2 and 4.3 depict the magnitude of the thigh and leg angle and the corresponding knee torque (for the same leg) during one period of the normal gait cycle (Winter, 2005). Each point is the mean of several tests for that specific percentage of stride and is called the sample mean of that stride.

As walking patterns differ between individuals, there are variations in data (Figures 4.2 and 4.3). Since the desired controller must provide the magnitude of the knee torque for the

prosthesis actuator, Figure 4.3 must be shifted by 50% to provide the value of the prosthetic knee torque; the result is shown by dash lines in Figures 4.4 and 4.5. The model is one that is based on control. The gait model is encoded using a Fuzzy Interference System (FIS). FIS is the process that formulates the mapping of a given input to an output, with fuzzy logic. The principle operation is one that measures the angle of the link segment models (femur and tibia) with respect to the ground, based on the component of gravity on each axis.

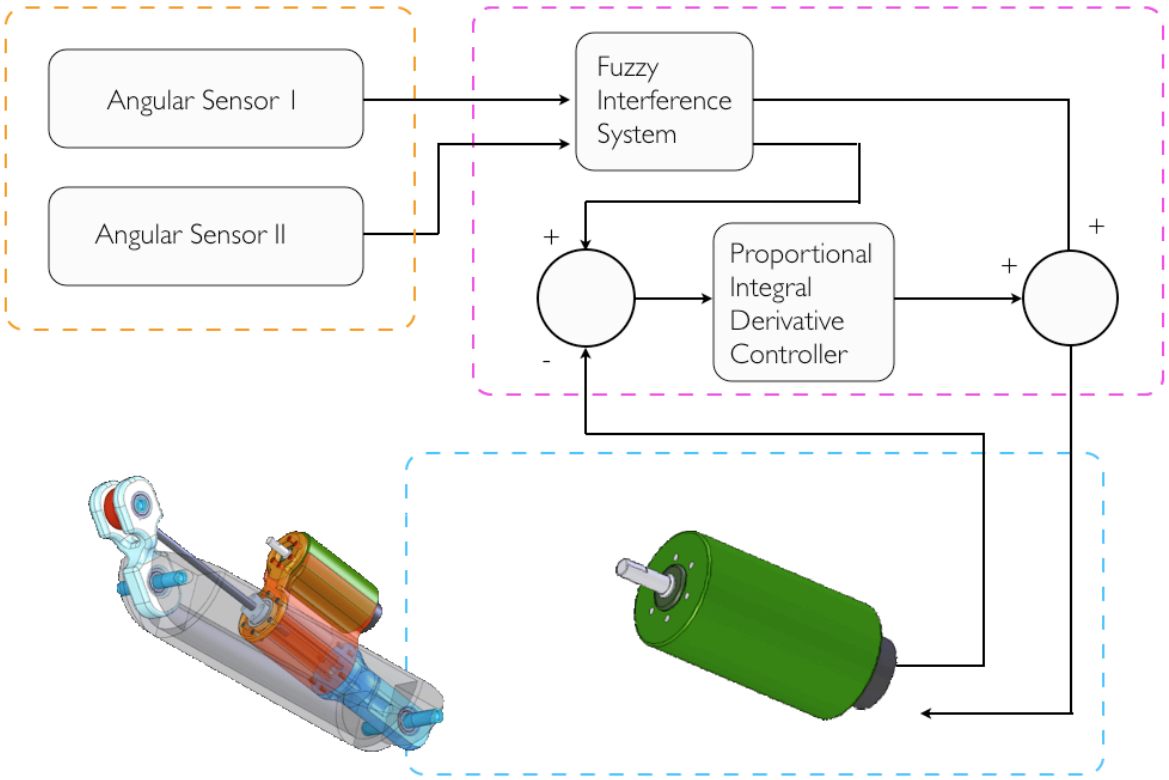

Figure 4.1: Control diagram of the APK

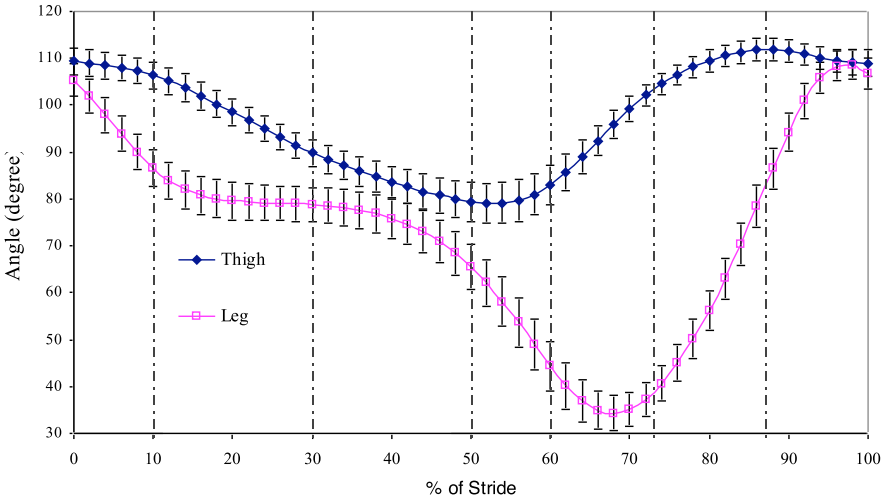

Figure 4.2: Thigh and leg angle for normal cadence

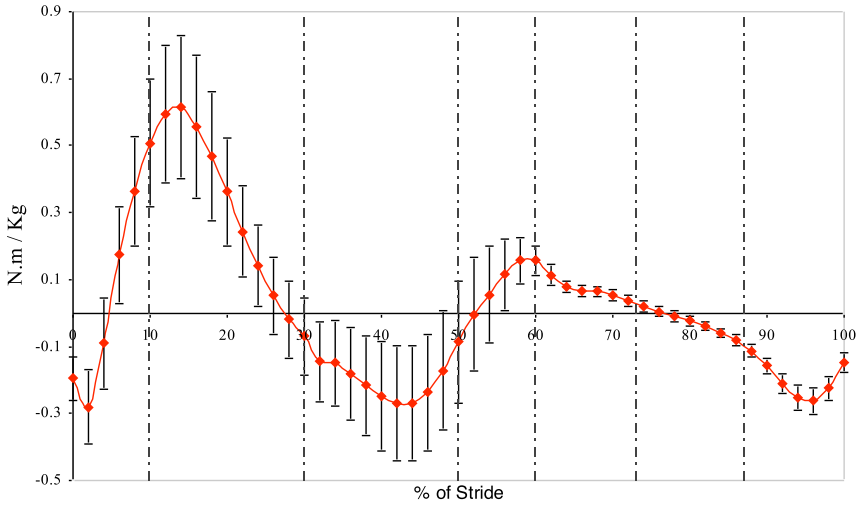

Figure 4.3: Knee torque for cadence

The control strategy in Figure 4.1 a new method of human gait phase recognition and cadence control. The proposed solution takes advantage of an Adaptive-Network-based Fuzzy Inference System (ANFIS) to control the knee torque as a function of echoing the angular state of the able leg (Jang, 1993). The rule-based system eliminates the need for the

mathematical model of the gait cycle during implementation of the control process. Moreover, fuzzy logic is suitable for experiments that utilize low-cost sensors.

4.2 Adaptive-Network-based Fuzzy Interference System

A type-1 Takagi-Sugeno-Kang (TSK) FIS described by fuzzy IF-THEN rules (Sugeno, 1988; Takagi, 1985) has found numerous practical applications in control, prediction, and inference. In a first order type-1 TSK model with a rule base of M rules, each having p antecedents, the lth rule can be declared as the follows:

$$\begin{aligned} R^l : \text{IF } x_1 \text{ is } F_1^l \text{ AND } \cdots \text{ AND } x_p \text{ is } F_p^l, \\ \text{THEN } y^l(\mathbf{x}) = c_0^l + c_1^l x_1 + c_2^l x_2 + \cdots + c_p^l x_p \end{aligned} \tag{4.1}$$

where $l = 1, \ldots, M$, c_j^l ($j = 0, 1, \ldots, p$) are the consequent parameters, $y^l(\mathbf{x})$ is the output of lth rule, and F_k^l ($k = 1, \ldots, p$) are type-1 antecedent fuzzy sets.

$$\begin{aligned} y_{\text{TSK},1}(\mathbf{x}) &= \sum_{l=1}^{M} \bar{f}^l(\mathbf{x})\, y^l(\mathbf{x}) = \frac{\sum_{l=1}^{M} f^l(\mathbf{x})\, y^l(\mathbf{x})}{\sum_{l=1}^{M} f^l(\mathbf{x})} \\ &= \frac{\sum_{l=1}^{M} f^l(\mathbf{x}) \left(c_0^l + c_1^l x_1 + c_2^l x_2 + \cdots + c_p^l x_p \right)}{\sum_{l=1}^{M} f^l(\mathbf{x})} \end{aligned} \tag{4.2}$$

where the $f^l(\mathbf{x})$ is the rule firing level, defined as

$$f^l(\mathbf{x}) = T_{k=1}^{p} \mu_{F_k^l}(x_k) \tag{4.3}$$

in which T denotes a t-norm (usually minimum or product) and $\mu_{F_k^l}(x_k)$ is the membership value of kth associated with the lth rule. Further, $\mathbf{x}$ denotes a specific input that is applied to the type-1 TSK FIS.

A type-1 TSK FIS can be considered as a network that is composed of five layers. Inputs of the FIS come into the first layer where the premise parameters are stored. Membership values of inputs are calculated and will be sent to the next layer. The second layer computes the firing

level of rules based on the defined t-norm. In the third layer, the ratio of each rule's firing level to the sum of all rules' firing levels will be calculated, and the results will launch the forth stage. The forth layer gives $\bar{f}^l(\mathbf{x})\, y^l(\mathbf{x})$ for each rule based on the accumulated consequent parameters in this layer. The fifth layer computes the overall output as a summation of all incoming signals. Training data is essentially the input data (from the tibia and femur) and the output data (the knee torque), which is used in the ANFIS network. In order to achieve the desired input-output mapping, the given training data are fed forward to the network, and consequent parameters at layer four are identified by the least square estimate. In the backward pass, while output parameters are fixed, the error rates propagate backwards and premise parameters are updated by the gradient descent (Jang, 1993).

4.3 Designing the Fuzzy Interference System (FIS)

The FIS developed in this thesis is a two input, one output mapping with the knee torque being the sole output for the purpose of implementing the control architecture in Figure 4.1. We need to extend the FIS to input two output systems in order to incorporate theta as a second output (input to the PID).

Vertical dash lines are used on Figures 4.2 and 4.3 to partition the repetitive input data. These lines are chosen based on phases and sub-phases of the human walking cycle described in section 4.2.2. If it is assumed that the distribution of data in each cluster is normal and independent, the input membership functions are Gaussian. To define the input parameters of the FIS, average and standard deviation of the data in each partition are calculated and called mean and standard deviation of the sample mean for the partition of interest. The maximum number of rules allowed for a FIS is equal to the product of the number of membership functions for each input. Hence, it is the case that with the angular position of the femur and tibia, with seven fuzzy sets, the maximum number of allowed rules will be 49. Moreover, since during a walking cycle the thigh and leg must be in the same phase at all times, the rules of the TSK fuzzy system are restricted to:

$$\mathrm{R}_i : \text{IF } \; x_1 \text{ is } \mathrm{Ph}_1^i \; \text{ AND } \; x_2 \text{ is } \mathrm{Ph}_2^i \; \text{ THEN } \; y = c_0^i + c_1^i x_1 + c_2^i x_2 \tag{4.4}$$

where x_1 and x_2 are input 1 (femoral angle) and input 2 (tibial angle) respectively; c_0^i, c_1^i, and c_2^i are consequent parameters, i =1,…, 7, and Ph_j^i corresponds to the phase number i for jth input. Therefore, the total number of rules becomes seven for the two-input system.

To measure the effect of the output at the previous time instance on the current output of the system, the structure of the fuzzy model was revised. For the comparison of the current states of each input with its last state, the premise will read as:

$$\text{IF} \quad x_j(k) \text{ is } \text{Ph}_j^i \quad \text{AND} \left(x_j(k-1) \text{ is } \text{Ph}_j^i \text{ OR } x_j(k-1) \text{ is } \text{Ph}_1^{i-1} \right) \tag{4.5}$$

where j is the input index, which can be 1 or 2. The above statement means that if the current state of input j is in phase i, the previous state of that input must be in the same phase or in the one prior. It is noted that the phase number "zero" is the same as phase number "seven" since the input is iterative. As described earlier, the femoral and tibial state at any time must be in the same phase; moreover the rules that use a mixture of "AND" and "OR" connectives can be decomposed into equivalent rules. As a result, the two successive rules of the new FIS can be expressed as:

$$\begin{aligned} \text{R}_l \quad : \ & \text{IF} \quad x_1(k) \text{ is } \text{Ph}_1^i \quad \text{AND} \quad x_1(k-1) \text{ is } \text{Ph}_1^{i-1} \quad \text{AND} \\ & \quad x_2(k) \text{ is } \text{Ph}_2^i \quad \text{AND} \quad x_2(k-1) \text{ is } \text{Ph}_2^{i-1} \\ & \text{THEN} \quad y^l = c_0^l + c_1^l x_1 + c_2^l x_2 + c_3^l x_3 + c_4^l x_4 \end{aligned} \tag{4.6}$$

$$\begin{aligned} \text{R}_{l+1} : \ & \text{IF} \quad x_1(k) \text{ is } \text{Ph}_1^i \quad \text{AND} \quad x_1(k-1) \text{ is } \text{Ph}_1^i \quad \text{AND} \\ & \quad x_2(k) \text{ is } \text{Ph}_2^i \quad \text{AND} \quad x_2(k-1) \text{ is } \text{Ph}_2^i \\ & \text{THEN} \quad y^{l+1} = c_0^{l+1} + c_1^{l+1} x_1 + c_2^{l+1} x_2 + c_3^{l+1} x_3 + c_4^{l+1} x_4 \end{aligned} \tag{4.7}$$

where (l and l+1) = (1 and 2), (3 and 4), …, (13 and 14); and $c_i^l = c_i^{l+1}$ (for i = 0, … ,4). $x_j(k)$ and $x_j(k-1)$ (for j=1 and 2) can be considered as separated inputs that are associated with the same variable: femur or tibia angle. Hence, the membership functions related to $x_j(k)$ and $x_j(k-1)$ are the same. Consequently, the FIS under consideration has four inputs, fourteen membership functions and fourteen rules.

The results in Figures 4.4 and 4.5 are for the scenarios in which the current and the former status data are in same or successive phases, respectively. These values were found and validated using MATLAB.

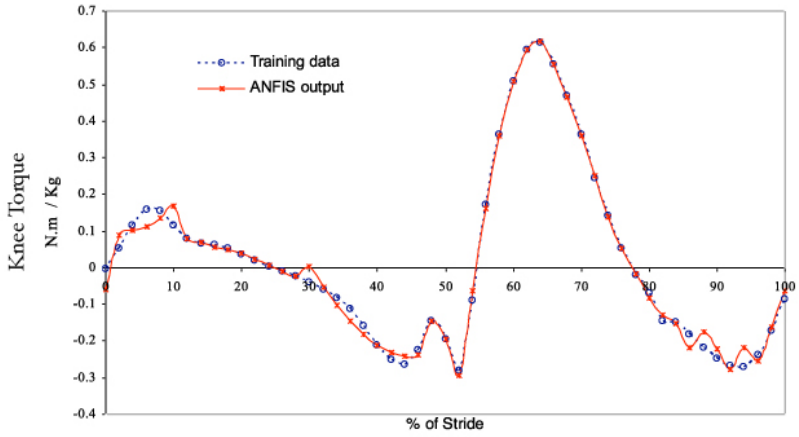

Figure 4.4: ANFIS output vs. training data, when the current and the former status of data are in the same phase

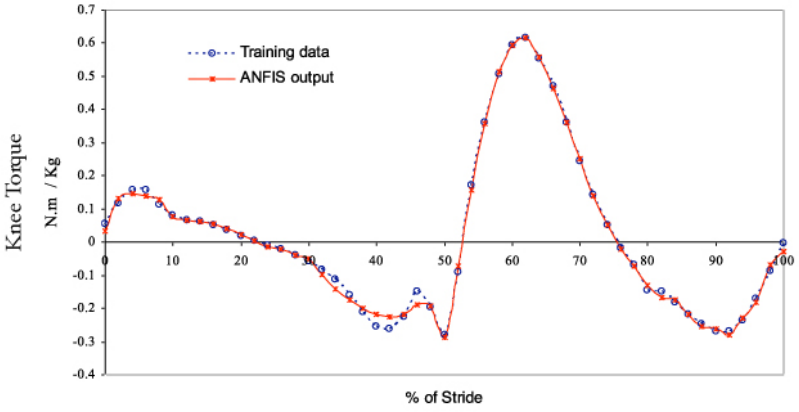

Figure 4.5: ANFIS output vs. training data, when the current and the former status of data are in successive phases

Chapter 5

Test Stand

5.1 Introduction

While concurrently developing the APK prototype, a test stand was designed and built to allow lower-limb motion experimentation. The experimental component is outside of the scope of this thesis. However, this thesis incorporates the design and development of the modular test stand. The purpose of the test stand is to replicate the entire gait motion, by allowing the motion from the greater trochanter (hip) to the metatarsals (foot) to follow the gait cycle. The test stand required two core components, a structural frame to hold the entire system erect, and a second system to simulate the motions of the femur. The total range of motion of the femur was set to +30° to -30° and was made possible using a long-stroke pneumatic cylinder. The preliminary design consisted of a device capable of mimicking both the femoral and tibial movements. Using a belt-pulley system connected to a electro-pneumatically controlled circuit allowed for accuracy, but due to exorbitant costs and strict timelines, could not be realized. A less expensive design was utilized and mated with the first prototype build. The test stand is a rigid, aluminum structure that allows for expansion.

5.2 Stand

The test stand is made from a Bosch Rexroth modular profile system, creating a rigid and durable frame. The aluminum structure allows the leg to swing freely with a total femoral range of motion of 60° (±30°) (Figures 5.1-5.2). Cross beams occupy the top, with a ⅛ inch Plexiglas® layer (Figure 5.3), allowing the electronic testing equipment to sit on. The femoral attachment linkages and corresponding pneumatic systems are integrated into the modular frame using bolts that slide into the Rexroth railing system.

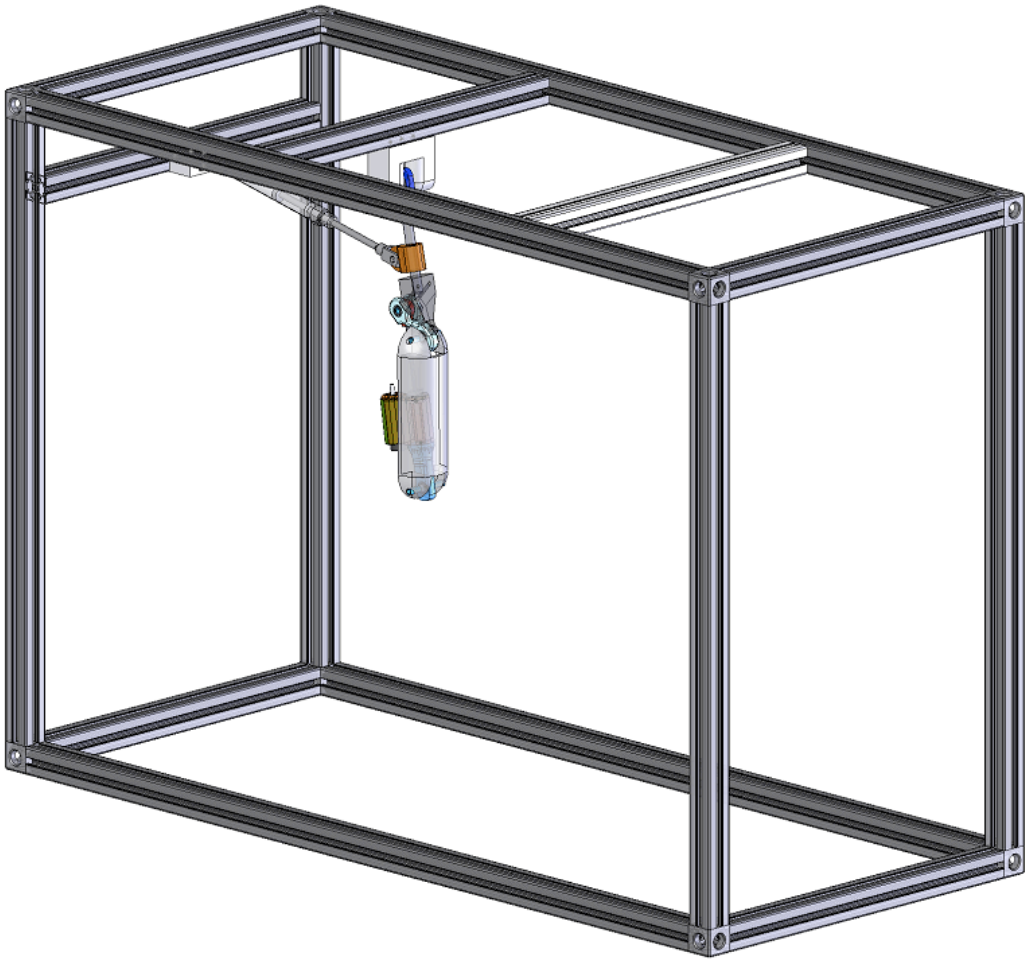

Figure 5.1: Modular test stand frame

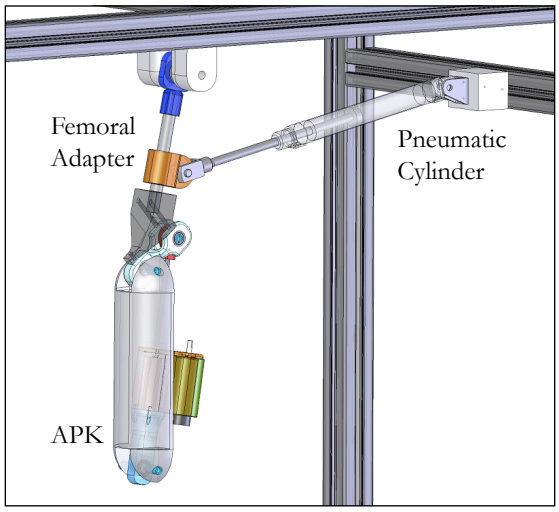

Figure 5.2: Modular test stand frame

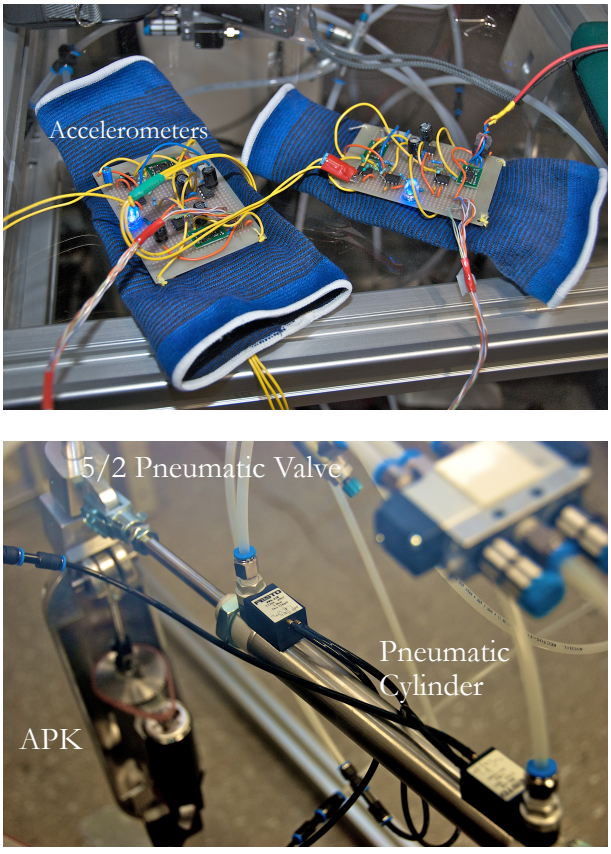

Figure 5.3: Plexiglas® top sheet acts as electronics and pneumatic carrier

5.3 Pneumatics

The pneumatically controlled system, as shown in Figure 5.4, is utilized for the mimicking of the femoral component. The femur link is connected to a cylinder with 160 mm of stroke travel. The circuit begins with a flow shut-off valve (1), allowing pressurized air to enter the system. The air progress onwards to a 5/2 valve (2), which is switch controlled based on the two 2/2 vales with a one-way spring activation (4). The 2/2 valves are necessary for automatic motion of the cylinder (5). The air pressure into the cylinder (5) is modulated by two one-way control valves (3). The one-way control valves (3) based on proper modulation can allow for varying gait speeds.

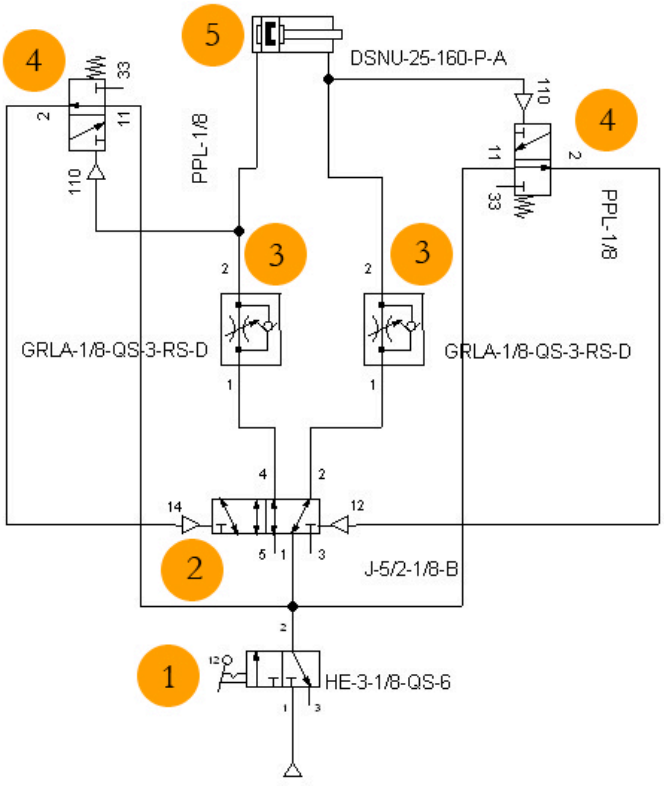

Figure 5.4: Pneumatic circuit

Figures 5.5 highlights the total range of motion of the femur. Figures 5.6 and 5.7 are images of the 2/2 and 5/2 values and the cylinder, respectively. The pneumatic system is shown to be integrated into the modular test stand frame.

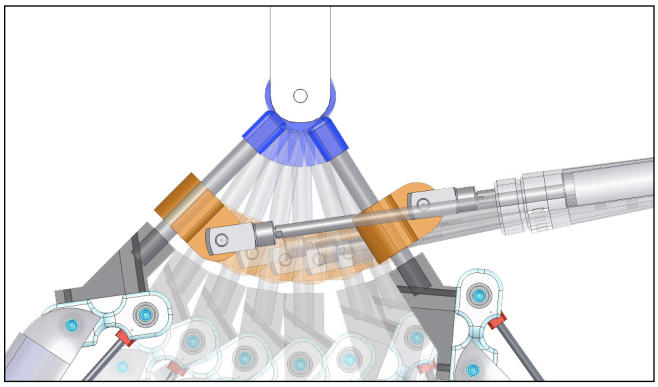

Figure 5.5: Pneumatic cylinder allows femoral range of motion of 60°

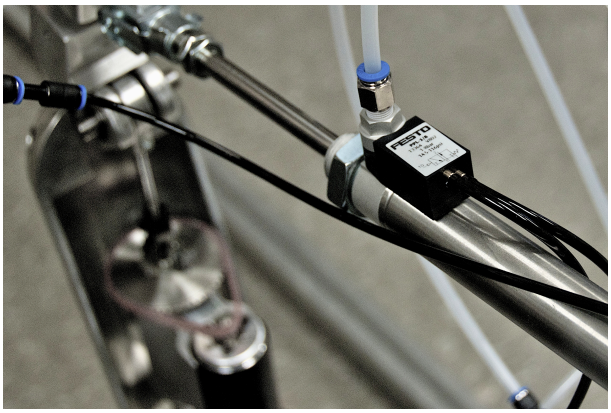

Figure 5.6: Pneumatic cylinder and 2/2 valve

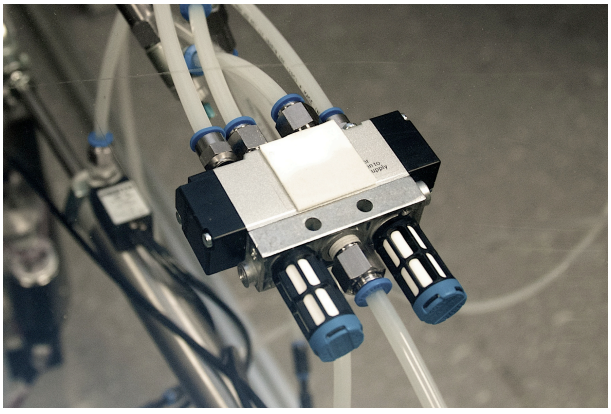

Figure 5.7: 5/2 pneumatic valve

5.4 Discussion

The test stand is an important feature of the overall APK prototype development, as it provides experimentation analysis. The modular design allows for greater future expansion as the studies progress further.

The main objective of the test stand is to provide experimentation of the APK with the addition of an attachment that replicates the motion of a femur. The gait cycle as reviewed in Chapter 2, finds that the greater trochanter (hip), the knee joint, ankle and metatarsals, move in a sinusoidal motion. In order to replicate these sinusoidal motions as well as place weight bearing experiment, further design additions must be made. Firstly, the sinusoidal motion of the hip can be adapted by placing a spring-based system to the femoral adapter (Figure 5.5). Secondly, on the same component, the design can be made such that it can have loads applied onto it, replicating upper body weight. These are two methods that will allow experimentation to be more realistic. Furthermore, the first iteration of the test stand is such that the leg is isolated away from any ground reaction force. By placing either a treadmill-based foundation or a low-friction floor, will allow the APK (with a foot attachment) to perform more realistic weight bearing tests.

Chapter 6

Conclusion and Future Work

6.1 Conclusion

The active prosthetic knee project has two fundamental objectives: firstly, to enable the user to increase walking efficiency by allowing the prosthetic to fully power the knee joint and secondly, to provide a low-cost, modular device. It is found that the mimicking of the knee's anatomical motion of 6-DOF is a near impossible feat to replicate with engineering mechanics. In this thesis, the design is simplified to a 1-DOF system (at the knee joint), that allows torque control to be modulated using a micro-controller. Having a mechanically simple system driven by precision controls allows the APK to be a an effective, low-cost prosthetic.

Throughout this research, we investigated the mechanical feasibility, designed and developed a novel idea into a prototype reality. Using a servomotor and unique gearing reductions, the artificial knee joint is able to generate an active torque to assist the user and to allow prolonged use. Various design trials included using gearbox and harmonic gear reductions, but due to their tremendous costs, was deemed inviable. Other methods such as polycentric knee designs,

and even hydraulically controlled knee joints were considered; however, the design process led us to the ball screw design.

Once the APK design study was complete, the research also delved into the finite element analysis study, to investigate the loading characteristics of the APK. Using mathematical models of compressive loads using real kinesiology data, it was found that the APK is mechanically resilient, although two core components, the knee torque arm and the ball screw can be more substantial in size. The current design may lead to plastic deformation, which is an undesired characteristic. The APK, based on our demographic study, is found to be lighter by approximately one kilogram compared to the anatomical leg.

By utilizing the gait data presented in Winter (2005), the knee angle versus percentage of gait cycle provides the necessary input values for the training data from the tibia and femur. The output values of the knee torque with the input values is used in the Adaptive-Network-based Fuzzy Interference System (ANFIS).

Lastly, the test stand is a rigid system with integrated features that allow motion to simulate lower-limb motions. The femur's motion is replicated with a pneumatic system, allowing various speeds and a maximum range of motion of 60°.

6.2 Future Work and Recommendations

The first APK prototype build is in the testing phases. As future developments continue to expand the prosthetic's capabilities, hardware updates should be considered. In other words, the following are identified as potential future directions:

1. The literature review investigated aspects of polycentric knee devices. It is recommended that incorporating a reinforcing secondary exoskeletal polycentric system braced around the original APK device may provide better structural stability.

2. The ball-screw system may prove to be too narrow. Hence, a customized, bulkier unit may provide greater stability. Furthermore, high precision is necessary in order to allow the mechanics to function properly. The APK prototype endured slight misalignments and slight wobbles were noted.

3. The test stand's modular design can provide load bearing tests. It is imperative that load testing is placed on the APK to replicate dynamic loading characteristics. A treadmill-based base or low friction ground will provide accurate load bearing attributes.

4. By using the test stand, it is imperative that more tests be conducted to validate the APK's performance. The tests should not be limited to constant velocity walking gait cycles, but further expanded to variable gait speed tests. Experiments that test standing and sitting as well as transitional motions is vital as well.

5. Once the test stand experimentation is complete, human testing would logically follow. A broad demographic range of test subjects with extensive lab-based testing will verify feasibility.

Appendix A

RE40 Graphite Brushed Motor

This appendix highlights the brushed servomotor that is used on the APK. The Maxon RE40 graphite brushed motor entire program is shown. The model chosen for the APK is the Order Number 148877.

RE 40 40 mm, Graphite Brushes, 150 Watt

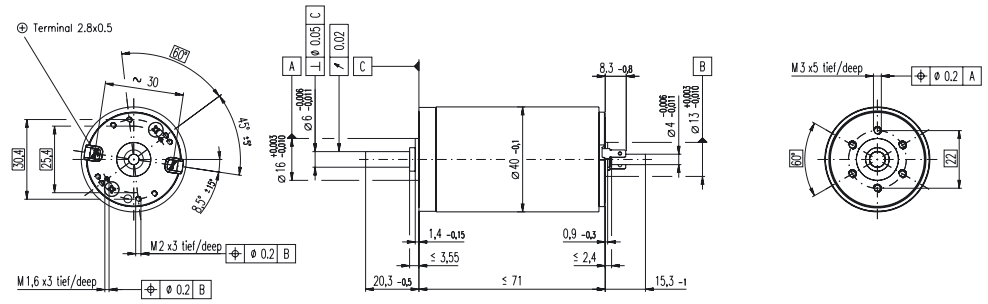

M 1:2

Stock program
Standard program
Special program (on request!)

			Order Number										
			148866	148867	148877	218008	218009	218010	218011	218012	218013	218014	218015
		Industrial version	263065	263066	263067	263068	263069	263070	263071	263072	263073	263074	263075
Motor Data													
1	Assigned power rating	W	150	150	150	150	150	150	150	150	150	150	150
2	Nominal voltage	Volt	12.0	24.0	48.0	48.0	48.0	48.0	48.0	48.0	48.0	48.0	48.0
3	No load speed	rpm	6920	7580	7580	6420	5560	3330	2690	2130	1710	1420	987
4	Stall torque	mNm	1690	2290	2500	1990	1580	996	796	641	512	415	289
5	Speed / torque gradient	rpm / mNm	4.11	3.32	3.04	3.23	3.53	3.36	3.39	3.35	3.37	3.44	3.45
6	No load current	mA	241	137	69	54	44	22	17	13	10	8	5
7	Starting current	A	103	75.9	41.4	28.0	19.2	7.26	4.69	3.00	1.92	1.29	0.627
8	Terminal resistance	Ohm	0.117	0.316	1.16	1.72	2.50	6.61	10.2	16.0	24.9	37.1	76.6
9	Max. permissible speed	rpm	8200	8200	8200	8200	8200	8200	8200	8200	8200	8200	8200
10	Max. continuous current	A	6.00	6.00	3.33	2.75	2.41	1.41	1.13	0.904	0.725	0.594	0.414
11	Max. continuous torque	mNm	98.7	181	201	196	198	193	192	193	193	191	190
12	Max. power output at nominal voltage	W	285	440	491	332	255	86.5	55.7	35.6	22.9	15.3	7.40
13	Max. efficiency	%	88	91	92	91	91	89	88	87	86	85	83
14	Torque constant	mNm / A	16.4	30.2	60.3	71.3	82.2	137	170	214	266	321	461
15	Speed constant	rpm / V	581	317	158	134	116	69.7	56.2	44.7	35.9	29.8	20.7
16	Mechanical time constant	ms	6	5	4	4	4	4	4	4	4	4	4
17	Rotor inertia	gcm²	135	134	134	125	127	118	117	118	117	114	114
18	Terminal inductance	mH	0.02	0.08	0.33	0.46	0.61	1.70	2.62	4.14	6.40	9.31	19.20
19	Thermal resistance housing-ambient	K / W	4.7	4.7	4.7	4.7	4.7	4.7	4.7	4.7	4.7	4.7	4.7
20	Thermal resistance rotor-housing	K / W	1.9	1.9	1.9	1.9	1.9	1.9	1.9	1.9	1.9	1.9	1.9
21	Thermal time constant winding	s	41	40	40	38	38	36	35	35	35	34	34

Specifications

Axial play	0.05 - 0.15 mm
Max. **ball bearing** loads	
axial (dynamic)	
not preloaded	5.6 N
preloaded	2.4 N
radial (5 mm from flange)	28 N
Force for press fits (static)	110 N
(static, shaft supported)	1200 N
Radial play **ball bearing**	0.025 mm
Ambient temperature range	-20 ... +100°C
Max. rotor temperature	+155°C
Number of commutator segments	13
Weight of motor	480 g
2 pole permanent magnet	

Values listed in the table are nominal.
For applicable tolerances see page 43.
For additional details please use the maxon selection program on the enclosed CD-ROM.

Operating Range

Comments Details on page 49

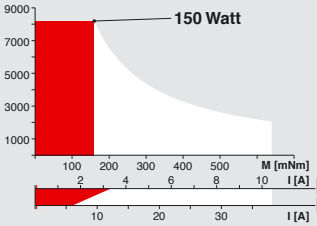

Recommended operating range

Continuous operation
In observation of above listed thermal resistances (lines 19 and 20) the maximum permissible rotor temperature will be reached during continuous operation at 25°C ambient.
= Thermal limit.

Short term operation
The motor may be briefly overloaded (recurring).

148877 Motor with high resistance winding
148866 Motor with low resistance winding

maxon Modular System

Overview on page 17 - 21

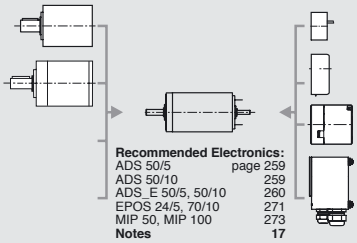

Planetary Gearhead
42 mm
3 - 15 Nm
Details page 224

Planetary Gearhead
52 mm
4 - 30 Nm
Details page 227

Recommended Electronics:

ADS 50/5	page 259
ADS 50/10	259
ADS_E 50/5, 50/10	260
EPOS 24/5, 70/10	271
MIP 50, MIP 100	273
Notes	17

Encoder MR
256 - 1024 CPT,
3 channels
Details page 239

Encoder HED_ 5540
500 CPT, 3 channels
Details page 242 / 244

Brake AB
40 mm,
24 VDC, 0.4 Nm
Details page 279

Industrial version
Encoder HEDL 9140
Details page 247
Brake AB
Details page 280

Figure A.1: RE40 Motor Program

Appendix B

Gait Data Analysis

This appendix presents the gait data of the lower body segment co-ordinates (Winter, 2005).

Table B.1: The gait data of the right knee, fibula and ankle co-ordinates (Winter, 2005)

Frame	**Time**	**Right Knee**		**Right Fibula**		**Right Ankle**	
	s	*x*	*y*	*x*	*y*	*x*	*y*
1	0.000	41.00	47.40	35.91	40.53	9.31	21.44
2	0.014	45.02	46.89	40.06	40.02	12.70	22.46
3	0.029	48.68	47.27	44.23	40.15	16.49	23.73
4	0.043	52.50	47.53	48.43	40.15	20.81	24.37
5	0.057	56.13	47.91	52.70	40.78	24.96	24.24
6	0.071	59.87	48.67	56.56	41.29	29.33	24.62
7	0.086	63.34	49.44	60.29	41.80	33.57	23.73
8	0.100	66.90	50.84	64.36	42.69	38.78	23.22
9	0.114	69.96	51.09	67.79	43.20	43.11	22.21
10	0.129	73.22	51.73	71.31	43.84	48.15	21.06
11	0.143	76.27	53.00	74.74	44.86	53.23	20.04
12	0.157	79.01	53.51	77.86	45.11	58.27	18.52
13	0.171	81.62	54.15	80.73	45.49	63.68	16.86
14	0.186	83.99	54.53	83.48	45.87	69.22	15.59
15	0.200	86.56	54.78	86.30	46.00	74.72	14.44
16	0.214	88.51	54.91	88.89	46.13	80.36	13.43
17	0.229	90.57	54.91	90.95	45.87	85.86	12.66
18	0.243	93.06	54.65	93.32	46.00	91.54	12.03
19	0.257	94.56	54.02	95.45	45.62	96.85	11.64
20	0.271	96.10	54.02	96.99	45.24	101.45	11.77
21	0.286	98.16	53.25	99.18	44.73	106.56	11.77
22	0.300	99.73	51.86	101.13	43.84	110.68	11.52
23	0.314	101.36	51.73	103.14	43.71	114.85	12.15
24	0.329	103.57	51.09	105.36	43.58	118.33	12.15
25	0.343	105.23	50.96	107.26	43.46	120.75	12.28
26	0.357	107.59	50.84	109.50	42.69	122.99	12.03
27	0.371	109.93	50.58	111.58	42.95	124.31	11.90
28	0.386	112.34	50.46	113.87	41.80	124.94	10.63
29	0.400	114.89	50.33	116.28	41.80	125.83	9.61
30	0.414	116.96	50.46	118.11	41.80	127.02	9.74
31	0.429	118.53	50.33	119.81	41.55	127.82	9.48
32	0.443	120.44	50.58	121.71	42.18	128.33	9.61
33	0.457	122.84	50.96	124.24	42.44	129.07	9.35
34	0.471	125.25	51.86	126.14	42.57	129.45	9.61
35	0.486	127.54	51.86	128.05	42.44	129.83	9.74
36	0.500	128.32	51.86	128.83	42.69	129.46	9.10
37	0.514	129.87	51.86	130.13	42.95	129.74	9.35
38	0.529	130.86	51.60	131.49	42.18	130.10	9.23
39	0.543	132.18	52.36	132.31	42.82	130.53	9.61
40	0.557	133.04	51.35	132.79	42.44	130.37	9.35
41	0.571	133.58	51.73	132.81	42.44	130.27	9.61
42	0.586	134.31	51.35	133.17	43.20	129.98	8.97

43	0.600	134.72	50.96	133.70	42.57	130.39	9.61
44	0.614	135.70	52.62	134.56	43.20	130.23	9.61
45	0.629	136.26	51.86	134.73	42.95	129.89	9.48
46	0.643	137.09	51.86	135.18	43.07	130.22	10.24
47	0.657	137.95	51.47	135.66	42.69	130.06	9.99
48	0.671	138.74	51.60	136.19	42.69	130.47	10.12
49	0.686	139.15	51.09	136.73	42.57	130.49	9.99
50	0.700	140.11	51.09	137.05	42.57	130.56	9.99
51	0.714	140.92	50.58	137.87	42.06	130.49	10.24
52	0.729	142.22	50.84	138.66	42.44	131.27	10.24
53	0.743	143.05	50.58	139.23	41.93	130.96	10.12
54	0.757	143.69	50.71	140.12	42.57	131.47	10.63
55	0.771	144.27	50.46	140.45	42.95	131.03	10.63
56	0.786	145.59	50.71	141.52	42.31	131.34	10.63
57	0.800	147.07	50.58	142.61	42.18	131.80	10.75
58	0.814	148.41	50.71	143.83	43.20	132.12	12.15
59	0.829	149.75	50.33	144.66	42.31	131.94	12.03
60	0.843	151.22	50.33	146.26	42.82	132.26	12.66
61	0.857	153.30	50.33	147.96	42.69	132.69	12.92
62	0.871	155.41	50.07	150.06	42.57	133.39	13.93
63	0.886	157.01	50.07	152.30	42.69	133.97	14.83
64	0.900	160.29	49.06	154.95	42.06	135.48	14.95
65	0.914	163.22	49.06	157.62	42.31	136.75	16.48
66	0.929	166.89	48.55	161.03	41.04	139.14	17.37
67	0.943	170.04	48.16	164.69	41.42	140.90	18.64
68	0.957	174.11	48.04	168.25	41.55	143.69	19.79
69	0.971	176.97	47.02	171.50	40.15	145.54	20.42
70	0.986	181.73	47.53	176.00	40.15	149.53	21.82
71	1.000	184.36	46.89	179.40	39.51	152.68	22.21
72	1.014	188.33	47.27	184.00	39.89	156.39	23.73
73	1.029	191.78	47.66	187.71	40.53	159.84	24.24
74	1.043	195.29	48.16	191.47	41.04	163.99	24.37
75	1.057	199.10	48.93	195.79	41.42	168.44	24.50
76	1.071	202.66	49.31	199.47	41.55	172.50	23.61
77	1.086	206.19	50.33	203.39	42.44	177.30	22.84
78	1.100	209.57	51.22	206.90	43.20	182.08	21.95
79	1.114	212.66	52.11	210.63	43.84	187.09	21.06
80	1.129	215.74	52.62	213.83	44.47	192.20	19.66
81	1.143	218.49	53.13	216.96	44.47	197.36	17.88
82	1.157	221.28	53.89	219.88	45.24	202.96	16.86
83	1.171	223.80	54.02	222.91	45.24	208.15	15.59
84	1.186	226.20	54.40	225.70	45.49	213.86	13.68
85	1.200	228.59	54.65	228.21	45.49	219.43	12.79
86	1.214	230.52	54.65	230.52	45.11	224.92	11.39
87	1.229	232.85	54.65	232.60	45.24	230.94	11.39
88	1.243	234.63	53.64	234.76	44.47	236.28	11.01
89	1.257	236.07	53.13	236.84	44.35	241.80	10.37
90	1.271	238.29	52.75	239.18	43.46	247.07	10.63
91	1.286	239.81	51.73	241.47	43.33	252.03	11.01

92	1.300	241.33	50.84	243.36	42.82	255.82	11.01
93	1.314	243.03	50.46	245.32	42.82	259.31	11.26
94	1.329	245.23	50.33	247.40	42.82	262.03	12.15
95	1.343	247.67	49.82	249.57	42.31	263.95	10.88
96	1.357	250.00	49.82	251.91	41.68	265.27	10.24
97	1.371	252.80	50.33	254.32	42.06	266.41	9.86
98	1.386	255.23	50.20	256.50	41.55	267.06	9.23
99	1.400	257.39	50.07	258.92	41.42	268.72	9.48
100	1.414	259.60	50.07	260.74	41.68	269.78	9.23
101	1.429	261.90	50.96	263.30	42.57	270.18	9.48
102	1.443	264.42	50.96	265.95	42.44	270.78	9.10
103	1.457	266.70	51.60	267.59	42.82	271.15	9.23
104	1.471	268.47	51.47	269.23	42.69	271.40	9.23
105	1.486	269.56	51.35	270.19	42.31	271.34	8.59
106	1.500	270.34	51.60	270.85	42.44	270.85	8.84

References

Alaranta H., Lempinen V.M., Haavisto E., Pohjolainen T., Hurri H. "Subjective benefits of energy storing prostheses." Prosthet Orthot Int. (1994);18 (2):92-97.

Ayyappa, Ed. "Normal Human Locomotion, Part 1: Basic Concepts and Terminology." JPO: Journal of Prosthetics and Orthotics (1997); 9: 10-17.

Bahler, Andre. "Fundamental Biomechanical Principles in the Orthotic Treatment of the Knee." JPO: Journal of Prosthetics and Orthotics (1992); 4: 157-165.

Blumentritt, Siegmar. "Design Principles, Biomechanical Data and Clinical Experience with a Polycentric Knee Offering Controlled Stance Phase Knee Flexion: A Preliminary Report." JPO: Journal of Prosthetics and Orthotics (1997); 9: 18-24.

Blumentritt, Siegmar. "Transfemoral Amputees Walking on a Rotary Hydraulic Prosthetic Knee Mechanism: A Preliminary Report." JPO: Journal of Prosthetics and Orthotics (1998); 10: 61-70.

Boonstra A.M., Schrama J.M., Eisma W.H., Hof A.L., Fidler V. "Gait analysis of transfemoral amputee patients using prostheses with two different knee joints." Archives of Physical Medicine and Rehabilitation (1996); 77 (5): 515-20.

Boonstra A.M., Schrama J.M., Fidler V., Eisma W.H. "Energy cost during ambulation in transfemoral amputees: a knee joint with a mechanical swing phase control vs. a knee joint with a pneumatic swing phase control." Scandinavian Journal of Rehabilitation Medicine (1995); 27 (2):77-81.

Breakey, James. "Beyond the Four-Bar Knee." JPO: Journal of Prosthetics and Orthotics (1998); 10: 77-80.

Buckley J.G., Spence W.D., Solomonidis S.E. "Energy cost of walking: comparison of intelligent prosthesis" with conventional mechanism. Archives of Physical Medicine and Rehabilitation (1997); 78 (3): 330-33.

"C-Leg Microprocessor Knee." OTTO BOCK Healthcare. 29 Aug 2007 <http://www.ottobockus.com/products/lower_limb_prosthetics/c-legproduct.asp>.

"CDC Growth Charts: United States – Stature-for-age percentiles: boys, 2 to 20 years." Centers for Disease Control and Prevention. May 30, 2000.

"CIA - The World Factbook -- Afghanistan." Central Intelligence Agency. April 28, 2008, <https://www.cia.gov/cia/publications/factbook/geos/af.html >.

English R.D., Hubbard W.A., McElroy G.K. "Establishment of consistent gait after fitting of new components." Journal of Rehabilitation Research and Development (1995); 2 (1): 32-35.

Frossard, Laurent. "Development and Preliminary Testing of a Device for the Direct Measurement of Forces and Moments in the Prosthetic Limb of Transfemoral Amputees during Activities of Daily Living." JPO: Journal of Prosthetics and Orthotics (2003); 15: 135-141.

Fujie, Hiromichi, Glen A. Livesay, Masahiro Fujita, and Savio L-Y. Woo. "Forces and Moments In Six-DOF at the Human Knee Joint: Mathematical Description for Control." Journal of Biomechanics (1996); 29 (12): 1577-1585.

Gailey R.S., Lawrence D., Burditt C., Spyropoulos P., Newell C., Nash M.S. "The CAT-CAM socket and quadrilateral socket: a comparison of energy cost during ambulation." Prosthet Orthot Int. (1993); 17 (2): 95-100.

Gard, Steven. "The effect of a shock-absorbing pylon on the gait of persons with unilateral transtibial amputation." Journal of Rehabilitation Research and Development (2003); 40: 109-124.

Gitter A., Czerniecki J., Meinders M. "Effect of prosthetic mass on swing phase work during above-knee amputee ambulation." American Journal of Physical and Medical Rehabilitation (1997); 76 (2): 114-21.

Godfrey C.M., Brett R, Jousse A.T. "Foot mass effect on gait in the prosthetic limb." Archives of Physical Medicine and Rehabilitation (1977); 58 (6): 268-69.

Greene, Peter. "A knee and ankle flexing hybrid orthosis for paraplegic ambulation." Medical Engineering & Physics (2003); 50: 539-545.

Haberman, Louis. "Silicone-Only Suspension (SOS) for the Above-Knee Amputee." JPO: Journal of Prosthetics and Orthotics (1992); 4: 76-85.

Hale S.A. "Analysis of the swing phase dynamics and muscular effort of the above-knee amputee for varying prosthetic shank loads." Prosthet Orthot Int. (1990); 14 (3): 125-35.

Hale, S.A. "The Effect of Walking Speed on the Joint Displacement Patterns and Forces and Moments Acting on the Above-Knee Amputee Prosthetic Leg." JPO: Journal of Prosthetics and Orthotics (1991); 3: 59-78.

Heller B.W., Datta D., Howitt J. "A pilot study comparing the cognitive demand of walking for transfemoral amputees using the Intelligent Prosthesis with that using conventionally damped knees." Clinical Rehabilitation (2000); 14 (5): 518-22.

Isakov E., Susak Z., Becker E. "Energy expenditure and cardiac response in above-knee amputees while using prostheses with open and locked knee mechanisms." Scandinavian Journal of Rehabilitation Medicine (1985); 12: 108-11.

Jacobs, Ron. "Mechanical Output From Individual Muscles During Explosive Leg Extensions: The Role of Biarticulate Muscles." Elsevier Science Ltd. (1996); 29: 513-523.

James K.B., Stein R.B. "Improved ankle-foot system for above-knee amputees." American Journal of Physical and Medical Rehabilitation (1986); 65(6): 301-14.

Jang J. "ANFIS: Adaptive-Network-based Fuzzy Interference Systems." IEEE Trans. Syst., Man, Cybern. (1993); 23 (3): 665-685.

Jarc, A.M. "The Design and Control of a Low-Power, Upper-Limb Prosthesis." IEEE (2006): 165-166.

Jergesen H.E., Hoaglund F.T., Roberts R.A., Wilson L.A., Lamoreux L.W., Radcliffe C.W.. "The University of California Biomechanics Laboratory four-bar polycentric knee linkage. A clinical trial in 20 active above-knee amputees." Clinical Orthopedics (1986); 204: 184-92.

Kapti, Akin. "Design and control of an active artificial knee joint." Mechanism and Machine Theory (2006); 41: 1477-1485.

Khan, Ismail. "Afghanistan one of the most affected countries." 07 Nov 1998. The News International. 29 Aug 2007 < http://www.rawa.org/mine2.htm>.

Li, Xue Mei, Bo Liu, Bo Deng, and Shi Ming Zhang. "Normal Six-Degree-of-Freedom Motion of Knee Joint During Level Walking." Journal of Biomedical Engineering (1996); 118: 258-261.

Macfarlane, P.A. "Transfemoral Amputee Physiological Requirements: Comparisons Between SACH Foot Walking and Flex-Foot Walking." Journal of Prosthetic & Orthotics (1997); 9: 138-143.

MacFarlane P.A., Nielsen D.H., Shurr D.G. "Mechanical gait analysis of transfemoral amputees: SACH foot versus the Flex-Foot." Journal of Prosthetics and Orthotics (1997); 9(4): 144-51.

MacFarlane P.A. Nielsen D.H., Shurr D.G., Meier K., Clark R., Kerns J., et al. "Transfemoral amputee physiological requirements: comparisons between SACH foot walking and Flex-Foot walking." Journal of Prosthetics and Orthotics (1997); 9: 138-43.

Maxon Motors 2005, Maxon RE40, 40 mm, Graphite Brushes, 150 Watt.

Menard M.R., McBride M.E., Sanderson D.J., Murray D.D. "Comparative biomechanical analysis of energy-storing prosthetic feet." Archives of Physical Medicine and Rehabilitation (1992); 73 (5): 451-58.

Murray M.P., Mollinger L.A., Sepic S.B., Gardner G.M., Linder M.T. "Gait patterns in above-knee amputee patients: hydraulic swing control vs. constant-friction knee components." Archives of Physical Medicine and Rehabilitation (1983); 64(8): 339-45.

Negoto, Yukio. "Development of Externally Powered Lower Limb Orthosis with Bilateral-servo Actuator." IEEE 9th International Conference on Rehabilitation Robotics (2005): 394-399.

Otto, Judith. "Prosthetic Knees: What's Currently New and Impressive?" The O&P EDGE. 29 Aug 2007 <http://www.oandp.com/edge/issues/articles/2003-10_03.asp>.

"Prosthetic Knee Joint Manufacturing in Vietnam." Prosthetics Outreach Foundation. 29 Aug 2007 <http://www.pofsea.org/knee.htm>.

Raade, Justin. "Analysis and Design of a Novel Hydraulic Power Source for Mobile Robots." IEEE Transactions on Automation Science and Engineering (2005); 2: 226-232.

Saito Y., Kikuchi K., Negoto, H., Oshima T., Haneyoshi T. "Development of Externally Powered Lower Limb Orthosis with Bilateral-servo Actual." Proceedings of the 2005 IEEE 9th International Conference on Rehabilitation Robotics (2005): 394-399.

Saunders J.B., Inman V.T., Eberhart H.D. "The major determinants in normal and pathological gait." The Journal of Bone and Joint Surgery (1953); 35-A: 543-58.

Sawicki, Gregory. "Powered Lower Limb Orthoses: Application in Motor Adaptation and Rehabilitation." IEEE 9th International Conference on Rehabilitation Robotics (2005): 206-211.

Schuch, C. Michael. "Thermoplastic Applications in Lower Extremity Prosthetics." JPO: Journal of Prosthetics and Orthotics (1991); 3: 1-8.

Skillings, Jonathan. "Prosthetics Go High Tech." 03 Aug 2003. CECS. 29 Aug 2007 <http://news.com.com/Prosthetics+go+high+tech/2008-1082_3-5816267.html>.

Stinus H. "Biomechanics and evaluation of the microprocessor-controlled C-Leg exoprosthesis knee joint." Z Orthop Ihre Grenzgeb (2000); 138(3): 278-82.

Sugeno M. "Structure identification of fuzzy model." Fuzzy Sets Syst. (1988); 23: 15-33.

Takagi T. "Fuzzy identification of system and its application to modeling and control." IEEE Trans. Syst., Man, Cybern. (1985); 15: 116-132.

The International Committee of the Red Cross (ICRC) Geneva, Orthopaedic Project in Afghanistan Fact Sheet, 2005.

Traugh G.H., Corcoran P.J., Reyes R.L. "Energy expenditure of ambulation in patients with above-knee amputations." Archives of Physical Medicine and Rehabilitation (1975); 56 (2): 67-71.

Van Der Linden M.L., Solomonidis S.E., Spence W.D., Ning Li, and Paul J.P., "A methodology for studying the effects of various types of prosthetic feet on the biomechanics of trans-femoral amputee gait." Journal of Biomechanics (1999); 32: 877-89.

Winter, David. Biomechanics and motor control of human movement. 3rd ed. John Wiley & Sons, Inc., 2005.

Yang L., Solomonidis S.E., Spence W.D., Paul J.P. "The influence of limb alignment on the gait of above- knee amputees." Journal of Biomechanics (1991); 24(11): 981-97.

Yousef Haik, Vinay Pai, Ching-Jen Chen, "Apparent viscosity of human blood in a high static magnetic field." Journal of Magnetism and Magnetic Materials (2001); 225: 180-186.

Zahedi, Saeed. "Adaptive prosthesis - a new concept in prosthetic knee control." Robotica (2005); 23: 337-344.

Zoss, Adam. "Biomechanical Design of the Berkeley Lower Extremity Exoskeleton (BLEEX)."IEEE/ASME Transactions on Mechatronics (2006); 11: 128-138.